# *Quantitative sequence stratigraphy applied to the Barremian–lower Aptian Urgonian carbonates deposited in Provence (southeastern France)*

**Mickaël Barbier, Jean Borgomano, Philippe Léonide, Gérard Massonnat, Charles Danquigny, and Jean-Louis Lesueur**

## ABSTRACT

Sequence stratigraphy is an essential tool for interpreting and predicting carbonate sedimentary systems architecture. The study explores an advanced quantitative stratigraphy method, which offers a new perspective compared to traditional sequence stratigraphy. The method is based on the correlation of increasing or decreasing trends of apparent accommodation calculated across sedimentary sections within a basin, supplemented by a new criterion: the bathymetry-to-thickness ratio to constrain the correlation and to replicate the stratigraphic architectures. This method has been applied to the Barremian–lower Aptian (Lower Cretaceous) Urgonian carbonate platform in Provence (southern France). Twelve major stratigraphic markers have been identified and correlated throughout the platform. Four major positive and negative apparent accommodation events were identified and correlated throughout the sedimentary profile, while eight minor events are locally highlighted. Major negative events were recognized specifically in outer-shelf domains and correlated with subaerially exposed units in shallower inner environments. Positive accommodation events are recorded in almost all locations of the carbonate sedimentary system. These findings provide a high-resolution, quantified stratigraphic framework, allowing us to assess the influence of tectonics and sea-level fluctuations on accommodation. This innovative approach offers



Manuscript received September 21, 2023; provisional acceptance January 17, 2024; revised manuscript received June 18, 2024; revised provisional acceptance August 5, 2024; second revised manuscript received December 18, 2024; final acceptance December 20, 2024.
DOI:10.1306/03182523084

## AUTHORS

MICKAËL BARBIER ~ *Centre Européen de Recherche et d'Enseignement de Géosciences de l'Environnement, Aix-Marseille Université, Aix-en-Provence, France; Akkodis France, Pau, France; mickael.barbier@akkodis.com*

Mickaël Barbier earned his Ph.D. in geosciences in 2012 from Aix Marseille University, France. His career spans roles in industrial and research-integrated projects aimed at understanding multiscale distribution of sedimentological, diagenetic, and structural heterogeneities in carbonate reservoirs. Currently at Akkodis, his expertise focuses on the characterization and three-dimensional modeling of carbonate reservoirs to provide advanced predictive modeling techniques.

JEAN BORGOMANO ~ *Centre Européen de Recherche et d'Enseignement de Géosciences de l'Environnement, Aix-Marseille Université, Aix-en-Provence, France; borgomano@cerege.fr*

Jean Borgomano earned his Ph.D. in carbonate geology in 1987 from Aix-Marseille University, France. He worked for Shell International as a carbonate geologist in exploration–production (1988–2003). As a professor, he led the Carbonate Reservoir Laboratory at Aix-Marseille University. He worked as a carbonate expert at Total (2013–2015) and then returned as a professor at Aix-Marseille University. His research focuses on the characterization and geological–numerical modeling of carbonate reservoirs.

PHILIPPE LÉONIDE ~ *Centre Européen de Recherche et d'Enseignement de Géosciences de l'Environnement, Aix-Marseille Université, Aix-en-Provence, France; leonide@cerege.fr*

Philippe Léonide earned his Ph.D. in sedimentology in 2007 from Aix-Marseille University. He joined the sedimentology and marine geology group at Vrije Universiteit Amsterdam (2009–2011). He is currently an assistant professor in carbonate sedimentology at Aix-Marseille University. His research focuses on the evolution of

carbonates through time, which have importance for the characterization of petrophysical properties in carbonate reservoirs.

GÉRARD MASSONNAT ~ *TotalEnergies, Pau, France; gerard.massonnat@totalenergies.com*

Gérard Massonnat earned his Ph.D. in hydrogeology and then graduated from IFP School in Petroleum Engineering and Project Development. After several positions in field monitoring, multidisciplinary studies, and research and development (R&D), he is presently an International Expert for Reservoir Geology and Geomodeling and R&D Fellow for TotalEnergies. His work now focuses on the development of the next generation of modeling tools for both matrix and dual porosity reservoirs.

CHARLES DANQUIGNY ~ *TotalEnergies, Pau, France; [4]Université Avignon, Campus Jean-Henri Fabre, Avignon, France; charles.danquigny@univ-avignon.fr*

Charles Danquigny obtained his Ph.D. in fluid mechanics in porous media from the University of Strasbourg (France) in 2003. He has been an associate professor at the University of Avignon (France) since 2006 and seconded to TotalEnergies since 2016. His research focuses on characterization and modeling of geological reservoirs, with a particular interest in predictive modeling of heterogeneity and upscaling.

JEAN-LOUIS LESUEUR ~ *TotalEnergies, Pau, France; jean-louis.lesueur@totalenergies.com*

Jean-Louis Lesueur earned his Ph.D. in lacustrine carbonate geology in 1991 from Bordeaux 3 University, France. With 18 years of experience abroad, he has held various roles including reservoir geology manager and geoscience manager. At headquarters, he served as deputy for reservoir geology, department deputy for geological specialties, and senior advisor for the exploration director. He joined the R&D entity 4 years ago.

robust tools to test scenarios of stratigraphic evolution and refine our understanding of carbonate platform dynamics.

## INTRODUCTION

Dynamic carbonate reservoir models are traditionally based on static geological frameworks derived from sequence stratigraphic well correlations, sedimentological interpretations, and an understanding of reservoir heterogeneities. Constructing carbonate stratigraphic architectures is a key step in carbonate sequence stratigraphy, especially for subsurface and reservoir modeling. Since the 1980s, sequence stratigraphy has been extensively used in both academia and the petroleum industry. It has proven invaluable for analyzing shallow-water carbonate sedimentary systems (e.g., Sarg, 1988; Handford and Loucks, 1993; Schlager, 1993, 2005; Pomar and Ward, 1995; Eberli et al., 2004; Droste, 2010; Catuneanu et al., 2011; Maurer et al., 2013; Pomar and Haq, 2016). This approach facilitates stratigraphic correlations across sedimentary basins and helps estimate influential factors such as sea-level changes and subsidence patterns.

However, recent research by Borgomano et al. (2020) highlights limitations in classical sequence stratigraphic models. To address these challenges, a quantitative carbonate sequence stratigraphic approach was developed. This method refines stratigraphic correlations and reduces uncertainties. It distinguishes between apparent accommodation and real accommodation. Real accommodation reflects the available sedimentary space over time, influenced by sea-level changes and subsidence relative to a fixed datum (Homewood et al., 2000). Apparent accommodation, in contrast, is inferred from measurable geological parameters, including facies bathymetry, bed thickness, and stratigraphic discontinuities. These measurements provide indirect insights into accommodation variations preserved in sedimentary records (Borgomano et al., 2020).

However, recent research by Borgomano et al. (2020) has underscored the limitations of classical sequence stratigraphic models, prompting the development of a new quantitative carbonate sequence stratigraphic approach to refine stratigraphic correlations and reduce associated uncertainties. It distinguishes between apparent accommodation and real accommodation. Real accommodation reflects the available space for sedimentation over time due to sea-level and subsidence changes relative to a fixed datum (Homewood et al., 2000). But neither sea level nor the subsidence is directly preserved as time-continuous and measurable variables in stratigraphic records. Apparent accommodation, in contrast, is inferred from measurable geological parameters, including facies bathymetry, bed thickness, and stratigraphic discontinuities. These measurements provide

indirect insights into accommodation variations preserved in sedimentary records (Borgomano et al., 2020).

The new method relies on calculating and correlating apparent accommodation trends across sedimentary sections to define stratigraphic architectures. These interpretations can be tested and refined through iterative forward modeling. Its utility is demonstrated by applying it to the well-documented Barremian to lower Aptian (Lower Cretaceous) Urgonian carbonates of Provence. This case study refines our understanding of stratigraphic architecture in these carbonates.

These carbonates are well exposed in southern France (Figure 1) and have been studied in detail during the last decades. Masse (1976) developed the first large-scale stratigraphic model, which was later updated (Masse, 1993). More recent work identified sedimentological and stratigraphical evidence of at least four Barremian to the lower Aptian drowning surfaces (Masse and Fenerci-Masse, 2011). Few existing high-resolution stratigraphic models mainly focus on horizontal and vertical dimensions of rudist beds and their relationships with coral bodies (e.g., Borgomano et al., 2002; Fenerci-Masse et al., 2005). Léonide et al. (2012) provided a first high-resolution stratigraphic architecture highlighting the spatial distribution of rudist-corals facies and adjacent outer-platform bioclastic sediments. Finally, Tendil et al. (2018) published a recent updated stratigraphic model based on platform to basin correlations of ammonite-calibrated timelines (Frau et al., 2018). This study provides a well-constrained chronostratigraphic framework for the definition of high-resolution stratigraphic architectures of the Barremian-lower Aptian Urgonian carbonates of Provence.

## GEOLOGICAL SETTINGS

### Geographic Location of Study Area

The current western Provence domain in southern France covers approximately 9000 km$^2$. It is bounded by the Durance River, the Sainte-Victoire structure, and the Arc syncline to the east; by the Mediterranean Sea to the south; by the Carpentras Basin and the Crau Plain to the west; and, finally, by the Ventoux-Lure structure to the north (Figure 1). The study area comprises, from north to south by the Plateau d'Albion (altitude ~850 m) and a series of east–west to northeast–southwest-trending folds and thrusts (La Nerthe, La Fare, Lubéron, and the Mont-Ventoux Lure structures). These are interrupted by north-northeast-trending strike-slip fault systems including the Nîmes, Salon-Cavaillon, Aix-en-Provence, and Mid-Durance faults (Tempier and Durand, 1981; Espurt et al., 2012).

During the Barremian to early Aptian, the study area was located at a paleolatitude of approximately 28°N. It constituted


## ACKNOWLEDGMENTS

The authors thank the reviewers for their invaluable contributions, which have significantly improved the quality of this paper. We also extend our gratitude to TotalEnergies for funding this R&D project and granting permission to publish this work.


## DATASHARE 202

Supplementary material is available in an electronic version on the AAPG website (www.aapg.org/datashare) as Datashare 202.

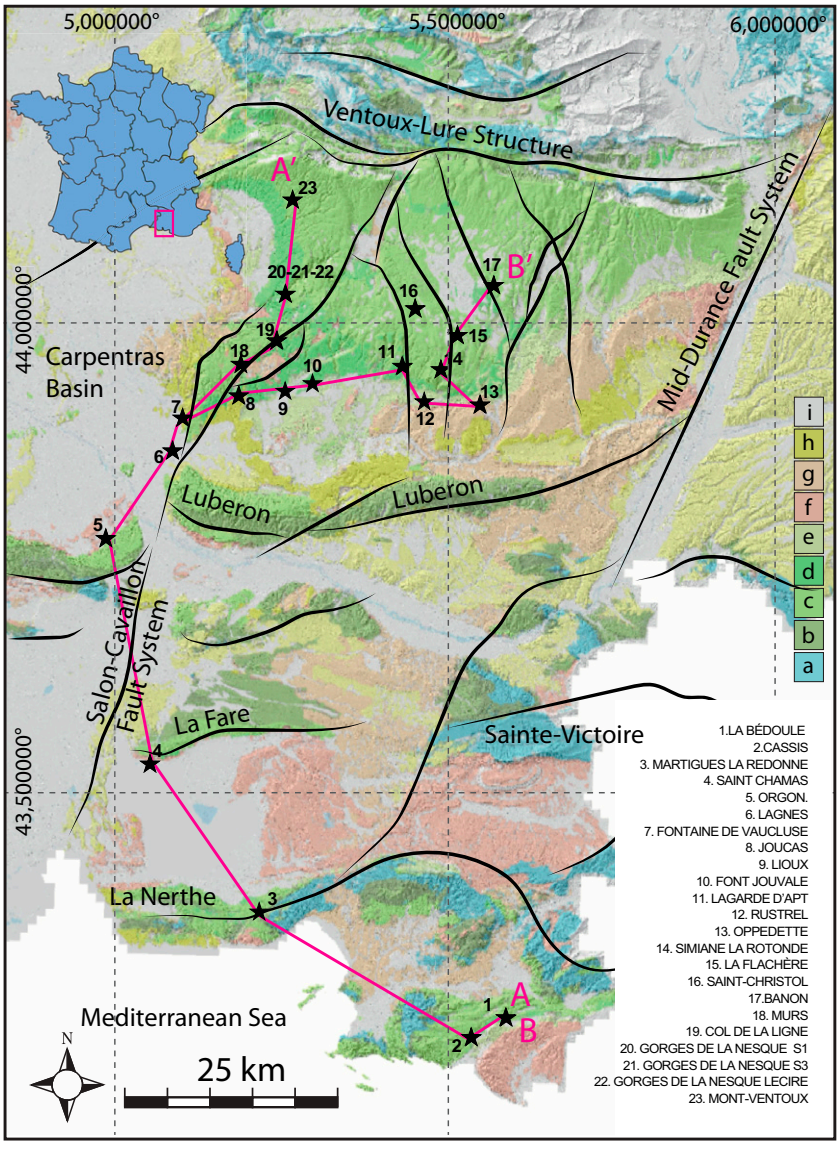


**Figure 1.** Localization of the study area, cross sections, and main sedimentary sections (black stars) studied in the present work. Dark lines correspond to major faults. a = Jurassic; b = Valanginian-Hauterivian; c = Barremian; d = lower Aptian; e = upper Aptian to Santonian; f = Eocene; g = Oligocene; h = Miocene; I = Quaternary. AA′ and BB′ are sedimentary cross sections in Figures 9–11.

the southern margin of the Vocontian Basin, where shallow-water carbonate platforms developed (Masse et al., 2000; Masse and Fenerci-Masse, 2013). This period is considered part of the Cretaceous greenhouse, during which sediments recorded significant fluctuations in the $\delta^{13}C$ curve, reflecting crises in primary productivity (Weissert and Erba, 2004). The mid-Barremian event, the Taxy event, and the early Aptian oceanic anoxic event (OAE1a) were reported to affect the carbonate production and sedimentation of the study area from the Barremian to early Aptian (Mutterlose et al., 2009; Huck et al., 2011, 2013; Tendil et al., 2018).

## Lithostratigraphy of the Urgonian Carbonates

The Barremian to lower Aptian Urgonian carbonates in Provence were previously studied by d'Orbigny (1850), Leenhardt (1883), Masse (1976), Léonide et al. (2012), and Tendil et al. (2018). The stratigraphic units defined by the above studies depend on the geographic location.

In southern Provence, the Urgonian carbonates are divided into three lithostratigraphic units (Figure 2). The Urgonian member is a 400- to 500-m thick limestone formation dated from the lower to upper

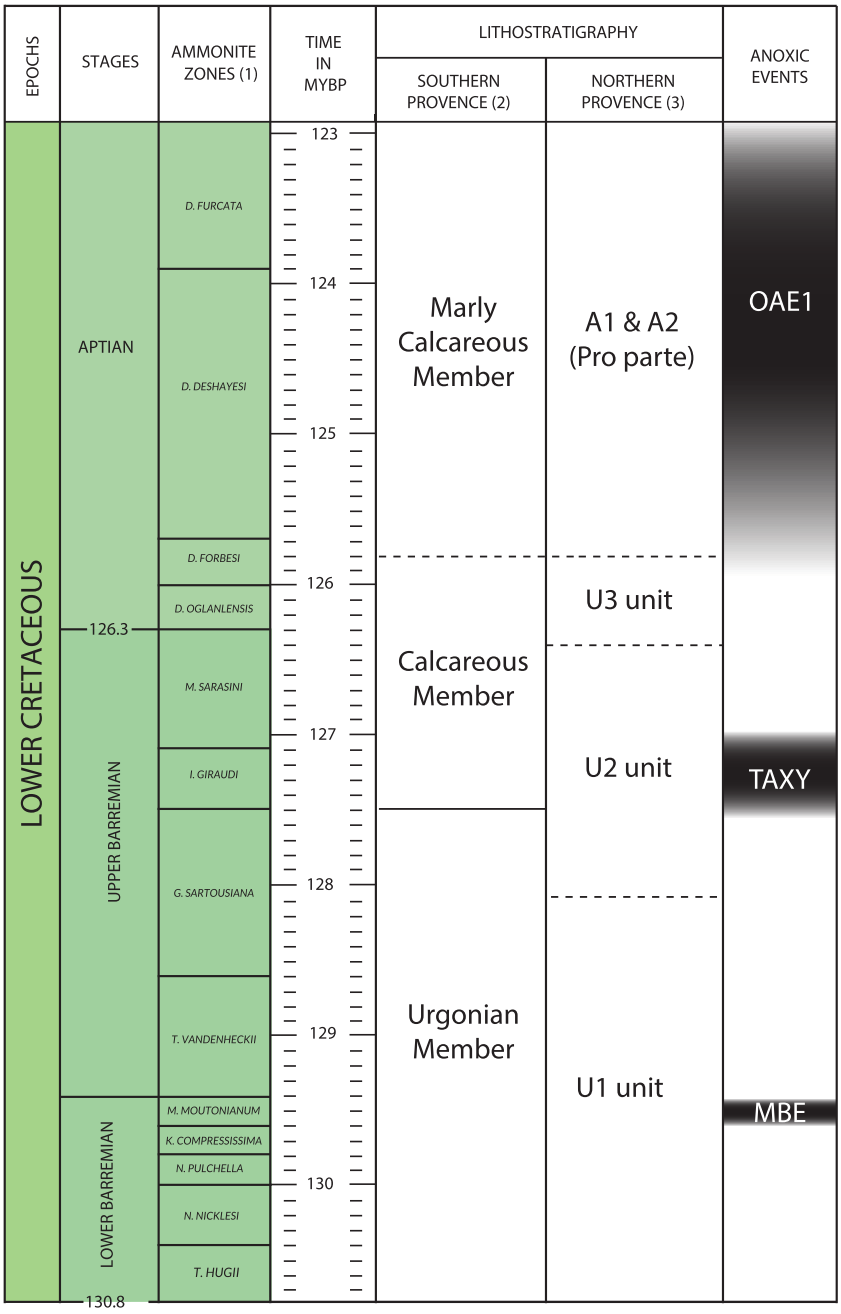


**Figure 2.** Modified from Tendil et al. (2018). The left half of the figure shows standard stratigraphic subdivisions calibrated to the absolute time scale and paleomagnetic reversal scale from Gradstein et al. (2012) associated with ammonite zones in southern and northern Provence. The right half displays the revised lithostratigraphic units of the Urgonian Provence platform for the Barremian/lower Aptian stages. (1) From Frau et al. (2018). (2) From Masse (1976) and Moullade et al. (2000). (3) From Leenhardt (1883) and Masse (1976). MBE = mid-Barremian event; MYBP = million years before present; OAE = ocean anoxic event; TAXY = Taxy event.

Barremian (Masse, 1976; Frau et al., 2018), characterized by massive rudist-bearing deposits. The overlying lithostratigraphic unit labeled the calcareous member by Moullade et al. (2000) is made up of alternations of upper Barremian to lower Aptian marls and limestones. Finally, the uppermost marly-calcareous member dated from the lower Aptian (Frau et al., 2015, 2018) is considered time equivalent to the OAE1a (Tendil et al., 2019).

In northern Provence, three Urgonian units were also defined (Leenhardt, 1883; Masse, 1976; Léonide et al., 2012; Tendil et al., 2018). The U1 unit is a

300- to 500-m-thick lower Barremian to basal upper Barremian unit, composed of cherty and bioclastic limestones. The U2 unit consists of a 50- to 250 m-thick rudist limestone formation dated to the upper Barremian. These last two units are time equivalent to the Urgonian and calcareous member in southern Provence. Finally, the U3 unit, dated from the lower Aptian, is faciologically equivalent to U1 and time-equivalent to the upper calcareous member in southern Provence.

## Urgonian Facies Model

The Urgonian sedimentological model has been the topic of many studies (Masse, 1976; Fenerci-Masse et al., 2005; Léonide et al., 2012; Masse and Fenerci-Masse, 2013). Fourteen facies associations have been defined and updated using macro- and micro-observations gathered from field, cores, and thin sections (Michel et al., 2023). This paper does not aim to provide a detailed description of each facies. We encourage the reader to refer to the above-cited papers for this purpose. However, all sedimentological criteria of the facies are described in detail in the supplementary material available as AAPG Datashare 202 at www.aapg.org/datashare. The facies model includes five main environments: inner platform, platform margin, outer platform, slope, and basin (Figure 3). According to Masse et al. (2011, 2013) and Tendil et al. (2018), the carbonate platform transitioned from a ramp to an extensive flat platform, spanning 100–140 km in

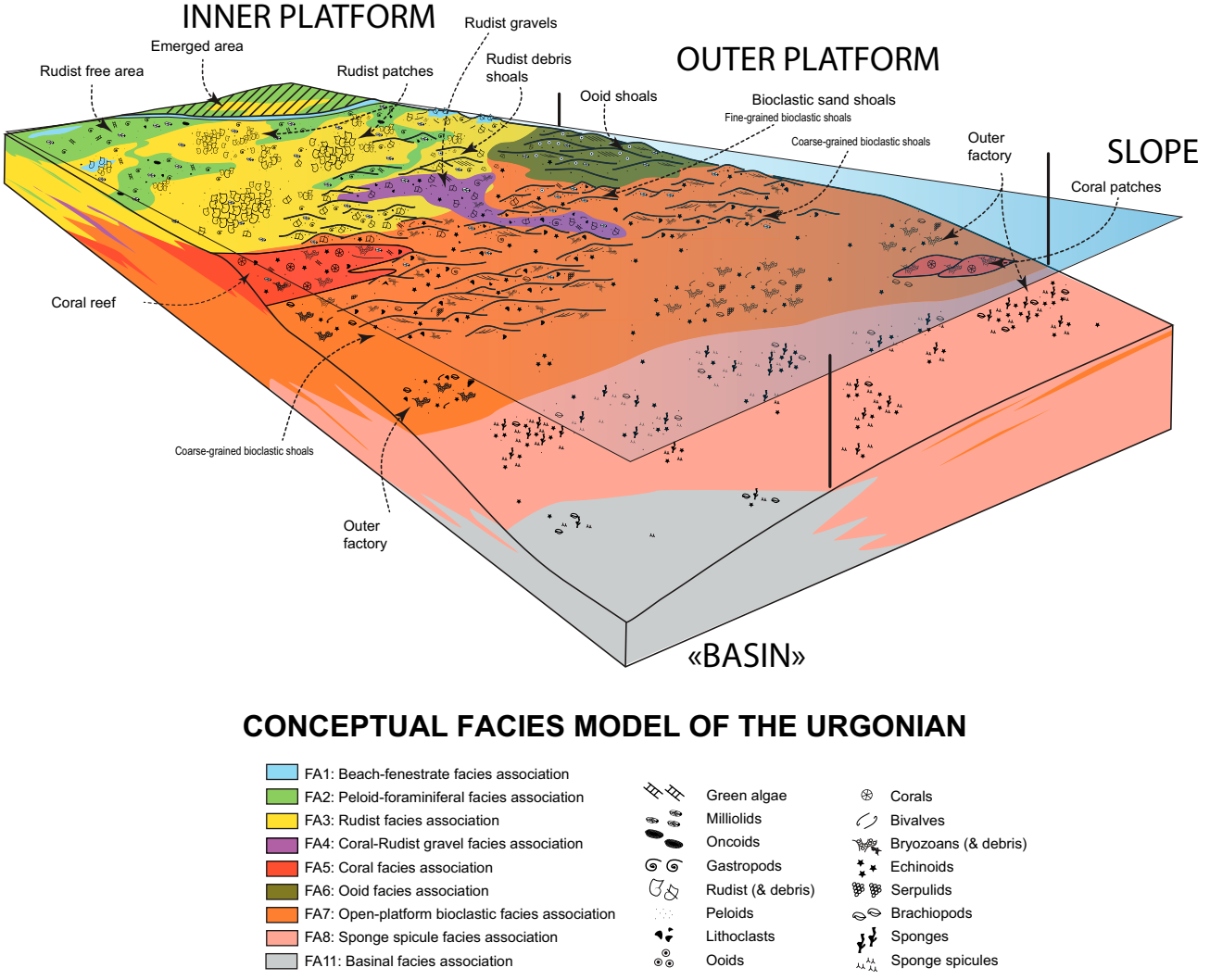


**Figure 3.** Facies model of the Urgonian carbonates from southeastern France.

length. By the late Barremian, it evolved into an isolated platform, restricted to northern Provence, with a reduced length of 30–60 km.

Beach-fenestrate grainstone (FA1), miliolid rich wackestone to grainstone (FA2), and rudist facies (FA3) are interpreted to deposit in the inner platform. The platform margin is characterized by coarse rudist and coral-bearing limestones (FA4) and kilometers-wide patches of coral wackestones to grainstones (FA5) (Masse, 1976; Masse et al., 2011; Léonide et al., 2012). Oolitic (FA6) and heterozoan-rich bioclastic (FA7) facies associations deposited in more open and higher-energy environments in with sediments transportation by wave currents and storm is a dominant process. The slope environment was characterized by reduced hydrodynamic energy and low light levels. It favors the deposition of fine to very fine bioclastic packstones to grainstones, grouped into FA8 and FA9. These facies contain abundant annelids, well-rounded echinoderm fragments, bryozoan debris derived from the outer platform, and sponge spicules.

The basin environment encompasses hemipelagic and pelagic facies. Hemipelagic deposits (FA10) are associated with fine-grained micritic limestones, whereas pelagic deposits (FA11) consist predominantly of marl-dominated lithologies (Masse, 1976; Léonide et al., 2012; Tendil et al., 2018). Finally, heterotrophic conditions are represented by FA13 and FA14. These correspond to gastropod-rich and *Palorbitolina*-rich wackestones to packstones, deposited on the platform and slope, respectively.

## DATA SET AND METHODS

The aim of this study is to test an alternative method for defining the stratigraphic architecture of carbonate sedimentary systems. The workflow is based on the spatial and temporal evolution of the facies water depth and quantified apparent accommodation changes combined with the classical analysis of stratigraphic surfaces.

### Calculation of Apparent Accommodation

Apparent accommodation is distinguished from real accommodation (Borgomano et al., 2020). The real accommodation represents in time the accommodation available created or destroyed from the evolution of both sea level (eustasy) and subsidence relative to a permanent datum (Borgomano et al., 2020). The apparent accommodation corresponds in depth to the preserved thickness of sediments added to the paleobathymetry for a given stratigraphic interval. This approach is rooted in the simple fact that neither sea level nor the subsidence is directly measurable in the stratigraphic record as a time variable. Facies paleobathymetry, bed thickness, porosity, and stratigraphic discontinuities are, on the contrary, directly measurable in the stratigraphic records and can thus be analyzed as indirect indications of real accommodation variations (Figure 4).

Calculated apparent accommodation is displayed for each sedimentary section as a cumulative curve with an uncertainty envelope related to the paleowater depth range. It is here calculated at each top of beds following the method proposed by Borgomano et al. (2020). Apparent accommodation (AAC) corresponds to the sum of (1) the cumulated compacted (uncompaction was not performed in this study) sediment thickness (CT) from the base of a sedimentary section and (2) the difference between facies water depth (WD) of the bed considered and the initial water depth (iWD).

$$\mathrm{AAC}\ (\mathrm{tn}) = \mathrm{CT}(\mathrm{from\ t0} \rightarrow \mathrm{tn}) + (\mathrm{WD}(\mathrm{tn}) - \mathrm{iWD}(\mathrm{t0}))$$

Consequently, values of apparent accommodation represent the evolution of the available space for sedimentation compared to the initial point, here referring to the base of a section. The finer the sedimentary descriptions are, the finer the vertical resolution of apparent accommodation is. Once the bathymetric and apparent accommodation curves have been built, increasing or decreasing trends emerge (Figure 4). A marker can then be placed at the interface between two different trends. Markers can be ranked according to the magnitude of the apparent changes.

### Calculation of the Bathymetry-to-Thickness Ratio

In classical sequence stratigraphic practices, deposition sequences are identified from the vertical stacking of sediments and correlated laterally between the different sections in a sedimentary basin. These sequences define two main fundamental criteria, which are the

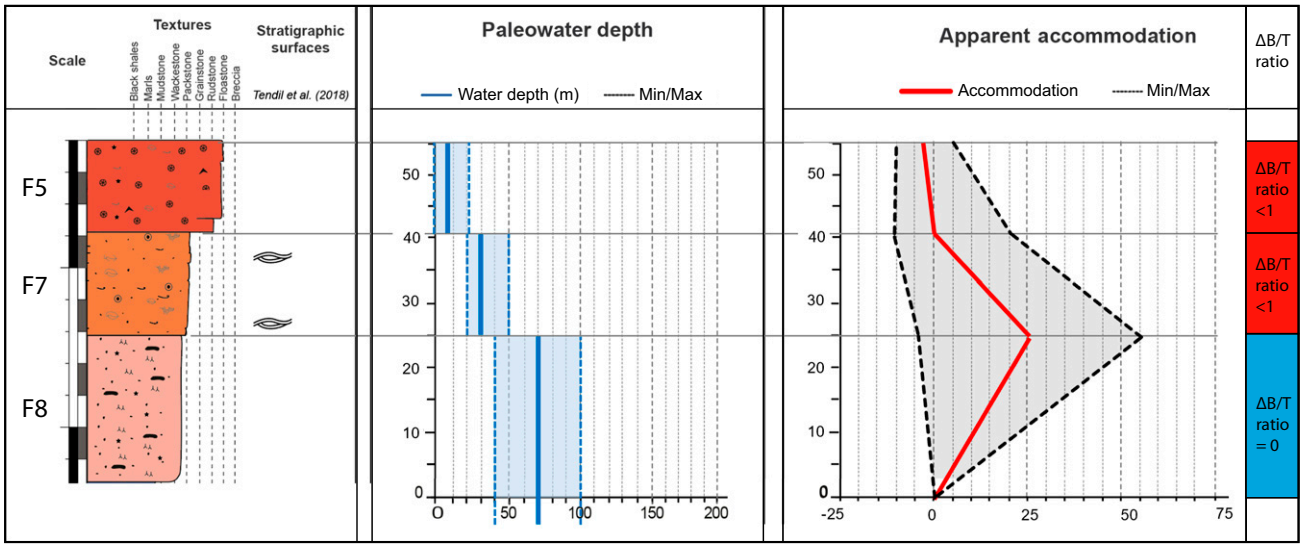


**Figure 4.** Method of apparent accommodation calculations. Step 1: Define the bathymetric ranges of facies (blue area). The bold blue line represents the most probable bathymetry. Step 2: Calculate the apparent accommodation at the top of each bed or facies change. This calculation includes the sum of the sediment thickness from the base and the bathymetric difference between facies and the initially defined water depth. The result is an apparent accommodation curve shown in red, with its uncertainty ranges indicated by the gray area. Refer to Figure 3 for the facies and component legend. The vertical scale of each section is the same. ΔB/T ratio = bathymetry-to-thickness ratio; Max = maximum; Min = minimum.

sediment supply and real accommodation, commonly represented by triangles. These triangles can have several meanings, according to the authors; however, in theory, they represent regressive and transgressive trends when the accommodation/sediment supply ratio (AAC/S) is less than one and AAC/S is greater than one, respectively.

In this work, we propose to correlate apparent accommodation trends laterally from one section to another, but with additional criteria such as the bathymetric variation over thickness ratio (ΔB/T) to reinforce the correlation hypothesis. The principle lies in the incremental analysis of variables used to calculate the apparent accommodation and to define the markers: the bathymetric variation between two markers divided by the thickness of the interval defined by the markers.

This ratio is powerful, as it can be interpreted in terms of sedimentary processes (regression, transgression, and sediment supply). Five cases can be encountered (Figure 5).

1. A ΔB/T ratio < −1 suggests a water-depth decrease higher than the interval thickness. This case involves a reduction of accommodation that could correspond to a forced regression and be followed by subaerially exposure. Such an interval may be capped by a type-1 sequence boundary sensu Schlager (2005).
2. A ΔB/T ratio = −1 corresponds to a water-depth decrease equivalent to the interval thickness. For instance, a 5-m-thick interval recording a bathymetric decrease of 5 m would have a ΔB/T = −1. In that case, no reduction of accommodation space is needed; the latter is filled only by the sediment supply. This condition describes progradation.
3. A ΔB/T ratio between −1 and 0 would suggest a water-depth decrease lower than the interval thickness. For instance, a 100-m-thick interval recording a water-depth decrease of −65 m would belong to this scenario. Accommodation space is filled faster than it is created, which consequently leads to a progressive decrease in water depths, defining a possible progradational pattern.
4. A ΔB/T = 0 ratio indicates an interval characterized by a constant water depth from base to top, independently of the thickness. The sediment supply is equivalent to the accommodation, indicating an aggrading pattern.

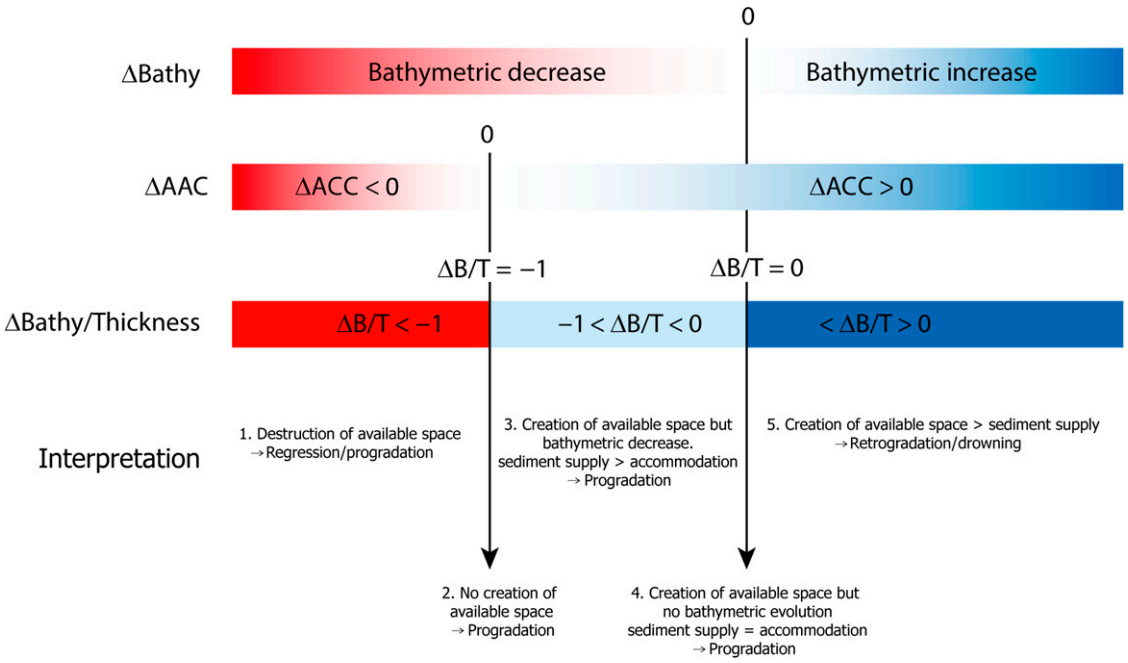


**Figure 5.** Definition and interpretation of the bathymetry-to-thickness ratio (ΔB/T). ΔAAC corresponds to the apparent accommodation differences between two markers.

The last three configurations would result in a type-2 sequence boundary sensu Schlager (2005).

5. A $\Delta B/T > 0$ ratio would, finally, indicate a water-depth increase independently of the thickness. The higher the $\Delta B/T > 0$, the higher the water-depth increase is recorded. It would clearly indicate an accommodation gain and a possible drowning process if the gain is important. This kind of ratio is associated with a vertical retrogradation pattern. Such an interval may be capped by a type-3 boundary sensu Schlager (2005).

Therefore, this ratio can help to quantify processes of apparent accommodation creation or destruction through time and space and is used together with the accommodation curve trends for correlating the sections through the study area.

## Facies and Water-Depth Attribution

In this study, the water depths of sedimentary facies are considered as input data for the calculation of apparent accommodation. These depths have been attributed to each facies based on interpretations from Purdy (1961), Hughes (2000), Hillgärtner et al. (2003), Masse et al. (2003), Immenhauser et al. (2004), Burla et al. (2008), Bover-Arnal et al. (2012), Bastide (2014), and Michel et al. (2023), who studied analogous sedimentary systems (Figure 6). Three water-depth categories were defined for each facies (see Table 1), representing the most probable depth, the minimum depth, and the maximum depth. The most probable depth corresponds to the most common bathymetry found for each facies, based on literature and field observations. It represents the depth at which the facies are most frequently encountered in analogous depositional systems. The minimum and maximum depths represent the uncertainty ranges for the bathymetric deposition of the facies. The minimum depth corresponds to the shallowest deposition depth recorded, whereas the maximum depth represents the deepest depth still consistent with the facies characteristics. These ranges are derived from both the geological literature and the known water-depth ranges of the producers and elements associated with each facies.

For instance, in Provence (France), Masse et al. (2003) and Fenerci-Masse et al. (2005) noted that rudist size increases with water depth. Their work suggested that muddy facies with small rudists were deposited in water depths of less than 1 m, whereas larger rudist-bearing grainy facies were found in the higher-energy subtidal zones of the platform interior,

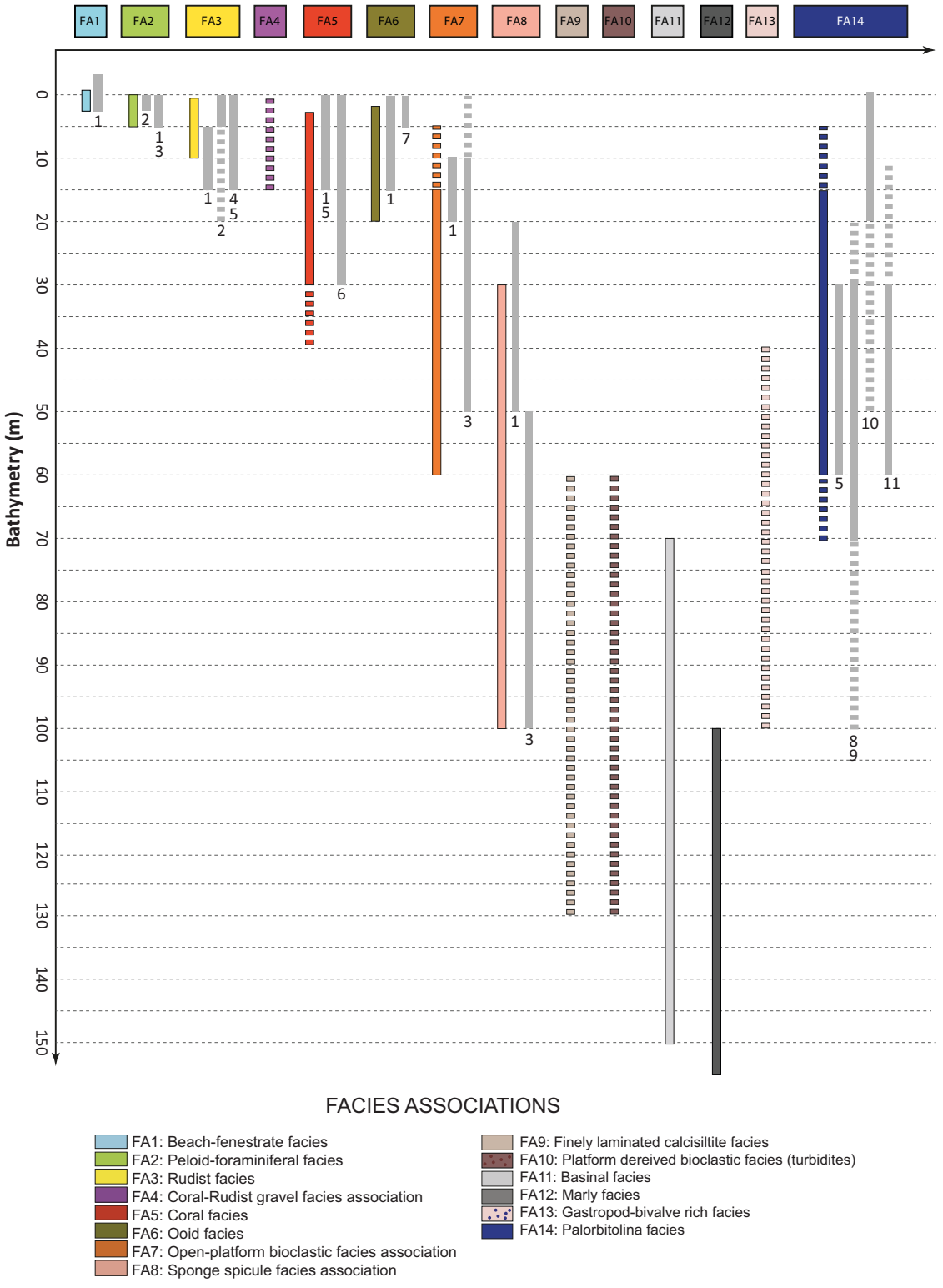


**Figure 6.** Graphical representation of the bathymetric range attributed to each facies associations and comparison with data from literature. Sources for bathymetry estimates: (1) Bastide (2014); (2) Masse et al. (2003); (3) Hillgärtner et al. (2003); (4) Burla et al. (2008); (5) Immenhauser et al. (2004); (6) Bover-Arnal et al. (2012); (7) Purdy (1961); (8) Masse (1976); (9) Rey and Cugny (1977); (10) Arnaud et al. (1998); (11) Hughes (2000).

**Table 1.** Water-Depth Ranges of Sedimentary Facies

| Facies Associations | | Water Depth (m) | | |
|---|---|---|---|---|
| FA | Facies Code | Most Probable | Minimum | Maximum |
| FA1 | 1a | 0 | 0 | 1 |
| | 1b | 0 | 0 | 1 |
| | 1c | 0 | 0 | 1 |
| | 1d | 0 | 0 | 1 |
| | 1e | 0 | 0 | 1 |
| | 1f | 0 | 0 | 1 |
| | 1g | 0 | 0 | 1 |
| FA2 | 2a | 0.3 | 0 | 3 |
| | 2b | 0.3 | 0 | 3 |
| | 2c | 0.2 | 0 | 3 |
| | 2d | 0.7 | 0 | 3 |
| | 2e | 0.7 | 0 | 3 |
| | 2f | 0.7 | 0 | 3 |
| | 2g | 0.7 | 0 | 5 |
| | 2h | 1 | 0 | 5 |
| | 2i | 2 | 0 | 5 |
| | 2j | 2 | 0 | 5 |
| | 2k | 2 | 0 | 5 |
| | 2l | 2 | 0 | 5 |
| FA3 | 3a | 0.3 | 0.2 | 3 |
| | 3b | 0.5 | 0.2 | 3 |
| | 3c | 1 | 0.5 | 5 |
| | 3d | 2 | 0.7 | 5 |
| | 3e | 5 | 3 | 10 |
| FA4 | 4a | 5 | 1 | 15 |
| FA5 | 5a | 10 | 3 | 30 |
| | 5b | 10 | 3 | 30 |
| | 5c | 8 | 3 | 20 |
| FA6 | 6a | 10 | 5 | 20 |
| | 6b | 10 | 5 | 20 |
| | 6c | 5 | 2 | 20 |
| FA7 | 7a | 30 | 25 | 60 |
| | 7b | 20 | 15 | 60 |
| | 7c | 20 | 15 | 60 |
| FA8 | 8a | 60 | 40 | 100 |
| | 8b | 50 | 30 | 90 |
| FA9 | 9 | 70 | 60 | 130 |
| FA10 | 10 | 70 | 60 | 130 |
| FA11 | 11 | 120 | 70 | 150 |
| FA12 | 12 | 150 | 100 | 200 |
| FA13 | 13 | 50 | 40 | 100 |
| FA14 | 14 | 50 | 5 | 70 |

where bathymetric depths ranged from 1 to 5 m. This interpretation is applied to FA3 (Table 1), where the most probable depth is assigned as 1–5 m. The assignment of water depths to all other facies follows a similar approach, based on depositional settings observed in the literature and the facies characteristics, including organism size, sediment texture, and hydrodynamic conditions. Although some uncertainty remains in the depth ranges, they are consistent with general trends observed in analogous environments and are supported by the available geological data.

## RESULTS

### Apparent Accommodation Calculation and Marker Identification

Apparent accommodation was calculated along each sedimentary section. The main evolutions obtained for Fontaine de Vaucluse (7 in Figure 1) and Martigues (3 in Figure 1) sections are shown below.

The Fontaine de Vaucluse section is 868 m thick and represents one of the most complete sections in the study area (lower Barremian to lower Aptian; Léonide et al., 2012; Frau et al., 2018). It required a positive cumulative apparent accommodation of +818 m to be formed, considering the section thickness and the facies water-depth difference (−40 m) between the base (70 m) and the top of the section (30 m) (Figure 7). The 300 first meters of the section are characterized by major changes of water depths, highlighting positive (P1/p2: uppercase = major event, lowercase = minor event) and negative apparent accommodation events (N1, n2, N3). For instance, the second interval formed in basin conditions during the early Barremian resulted from a positive apparent accommodation estimated at +234.5 m and, thus, a $\Delta B/T > 0$ (P2, Figure 7). The base of the upper Barremian (*Toxaster vandeheckii* ammonite subzone) displays a shallowing upward trend with a decrease of water depth approximately −50 m recorded along a 200-m-thick interval, which resulted thus from a positive accommodation pattern ($-1 < \Delta B/T < 0$). Above, the trend is different. Four cycles of both water depth and apparent accommodation (from p5 to N7 in Figure 7) are clearly observed. Accommodation decrease during N7 is estimated at −57 m. On the contrary, the first overlying rudist unit deposited in an invariable positive accommodation pattern characterizing a $\Delta B/T = 0$. This trend changes suddenly during the *Imerites giraudi* ammonite subzone, which was characterized by a drastic positive accommodation event (+88.5 m P9 in Figure 7), subsequently followed by a negative one, the overall being recorded along a 30-m-thick interval only (n8, Figure 7). Like previously, the second rudist unit formed during a constant positive accommodation context ($\Delta B/T = 0$) during the end of the Barremian. Finally, the top of the Fontaine de Vaucluse section displays a last long-term bathymetric rise and fall, emphasizing a positive and then negative evolution of apparent accommodation in the early Aptian.

The Martigues section consists of 415-m-thick Hauterivian to lower Aptian carbonates (Masse, 1976; Frau et al., 2018). It required a positive accommodation of +445 m to be formed that is almost half of the apparent accommodation recorded at Fontaine de Vaucluse (Figure 8). The Hauterivian–Barremian transition was marked by a drastic bathymetric decrease, emphasizing an intense negative accommodation ($\Delta B/T < 0$, N1 in Figure 8). Two cycles of water depth are recognized within the lower Barremian, but contrary to Fontaine de Vaucluse, the apparent accommodation is constantly positive ($\Delta B/T$ either $< 0$ or $> 0$ depending on the bathymetric evolution). The end of the early Barremian was marked by the exposure of the inner platform (Figure 8). At the beginning of the late Barremian (*T. vandeheckii* ammonite zone), aggradation of the inner platform occurred, resulting thus from a positive accommodation. Above, like at Fontaine de Vaucluse, the trend is different. Here, three cycles (instead of four at Fontaine de Vaucluse) of apparent accommodation are observed and involved three open-marine incursions onto the inner platform (from p5 to N7 in Figure 8). The top of the last negative apparent accommodation (−30 m) event (N7) was marked by exposure of the platform and the development of a paleosol. The overlying deposits characterized once again the aggradation of the inner platform in a positive accommodation context ($\Delta B/T = 0$) (Figure 8). A drastic increase of apparent accommodation (+90 m, P9) leading to bathymetric rise was recorded during the end of the late Barremian, whereas shallower settings returned to northern Provence during the same time interval. The subsequent deep basin settings prevailed in the early Aptian.

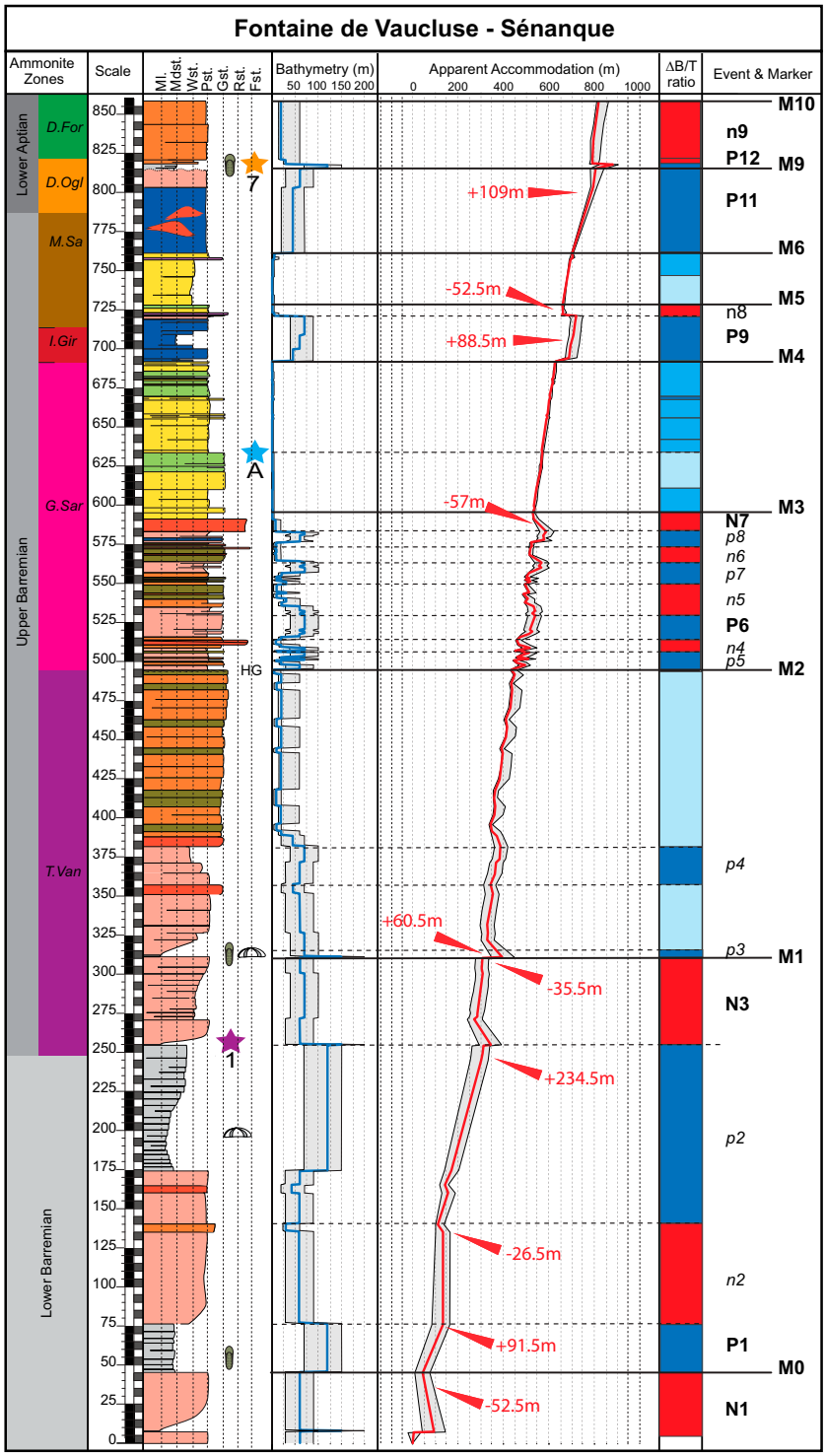


**Figure 7.** Updated Fontaine de Vaucluse sedimentary section and corresponding ammonite zones modified from Frau et al. (2018). Evolution of bathymetric facies ranges (blue line), apparent accommodation (red line), and bathymetry-to-thickness ratio (ΔB/T) are shown. Gray envelopes correspond to uncertainties. See Figure 5 for ΔB/T color legend, and refer to Figure 3 for the facies and component legend. Star 1 and 7 = bioevents 1 and 7 from Frau et al. (2018). Star A = last occurrence of *Agriopleura*. Uppercase = major event; lowercase = minor event. D.For = *Deshayesites forbesi*; D.Ogl = *Deshayesites oglanlensis*; E = exposure; Fst. = floatstone; G.Sar = *Gerhardtia sartousiana*; Gst. = grainstone; HG = hardground; I.Gir = *Imerites giraudi*; Mdst. = mudstone; Ml. = marl; M.Sa = *Martelites sartousiana*; N = negative accommodation event; P = positive accommodation event; Pst. = packstone; Rst. = rudstone; T.Van = *Toxancyloceras vandenheckii*; Wst. = wackestone.

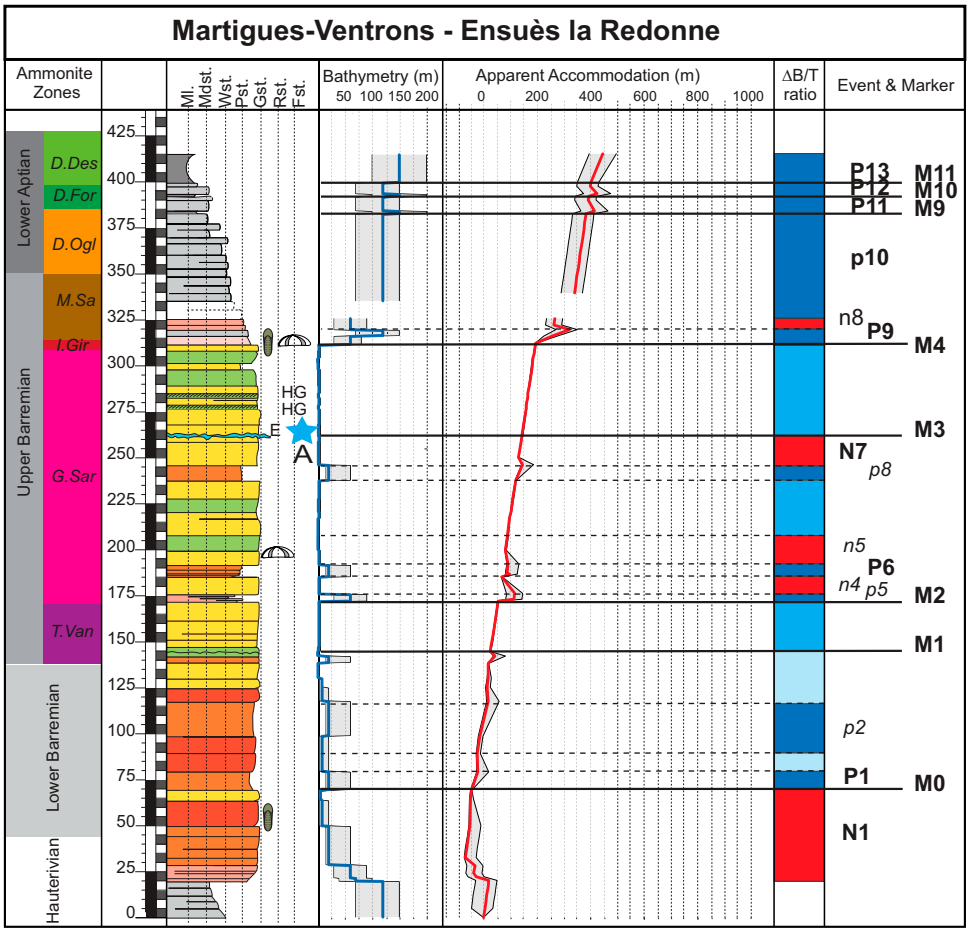


**Figure 8.** Updated Martigues-Ventrons sedimentary section and corresponding ammonite zones modified from Frau et al. (2018). Evolution of bathymetric facies ranges (blue line), apparent accommodation (red line), and bathymetry-to-thickness ratio (ΔB/T) are shown. Gray envelopes correspond to uncertainties. See Figure 5 for ΔB/T color legend, and refer to Figure 3 for the facies and component legend. Star A = Last occurrence of *Agriopleura*. Uppercase = major event; lowercase = minor event. D.Des = *Deshayesites deshayesi*; D.For = *Deshayesites forbesi*; D.Ogl = *Deshayesites oglanlensis*; E = exposure; Fst. = floatstone; G.Sar = *Gerhardtia sartousiana*; Gst. = grainstone; HG = Hardground; I.Gir = *Imerites giraudi*; Mdst. = mudstone; Ml. = marl; M.Sa = *Martelites sartousiana*; N = negative accommodation event; P = positive accommodation event; Pst. = packstone; Rst. = rudstone; T.Van = *Toxancyloceras vandenheckii*; Wst. = wackestone.

## Correlation of Apparent Accommodation Trends and Marker Identification

Twelve major markers of apparent accommodation variations have been defined and then correlated between the different sections of study area (Figure 9). This correlation has been carried out within chronostratigraphic framework defined by Masse (1976) and Frau et al. (2018) and modified in this study by updated descriptions.

### M0 Marker

A first negative apparent accommodation event (N1, $\Delta B/T < -1$) dated from the base of lower Barremian recognized at Martigues (3 in Figure 1) and Fontaine de Vaucluse (FdV; 7 in Figure 1) can be easily correlated at Orgon (5 in Figure 1; Figure 10). Its top defines the M0 marker. At Cassis (2 in Figure 1), M0 is placed at the uppermost part of an aggrading FA2 rich interval showcasing evidence of subaerial exposure (Masse, 1976). Above M0, a cyclic evolution of water depths and apparent accommodations (from P1 to N3 events) is discernible in southern and northern Provence, marking a change in the accommodation trends.

### M1 Marker

The M1 marker marks the end of the cyclic evolution. In northern Provence, M1 corresponds to the top of a negative apparent accommodation event (N3),

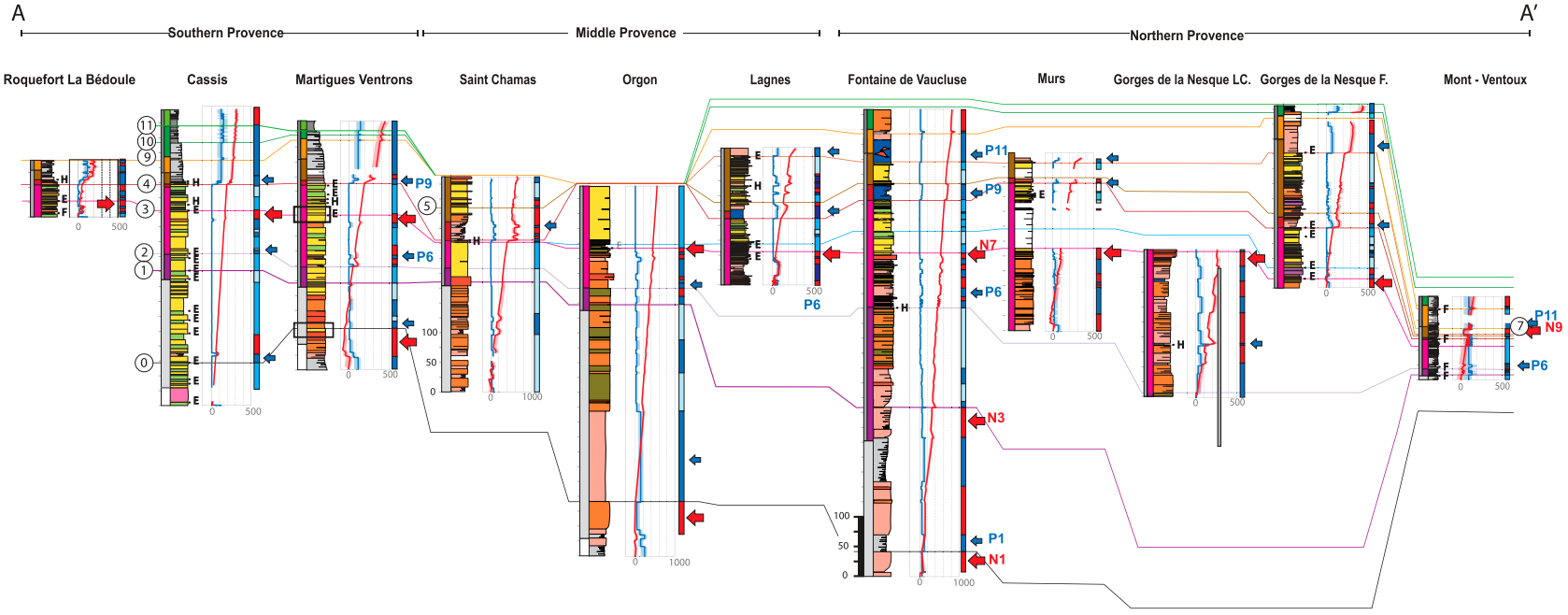


**Figure 9.** Correlation profile of the bathymetric and AA′ evolution from southern Provence to the western part of the northern Provence. See Figure 1 for location of the cross section. Ammonite zone dating and bathymetry-to-thickness ratio (ΔB/T) are also indicated. Surface numbers (black circles) correspond to marker number. Vertical scale is given along Saint Chamas sedimentary section. The black rectangles indicate the stratigraphic locations of the pictures shown in Figure 9. See Figure 3 for facies legend. Uppercase = major event; lowercase = minor event. E = exposure surface; F = firmground; Gorges de la Nesque F. = Gorges de la Nesque Fayol; Gorges de la Nesque LC. = Gorges de la Nesque Le Cire (see Léonide et al., 2012); H = hardground. N = negative accommodation events (red arrows); P = positive accommodation events (blue arrows).

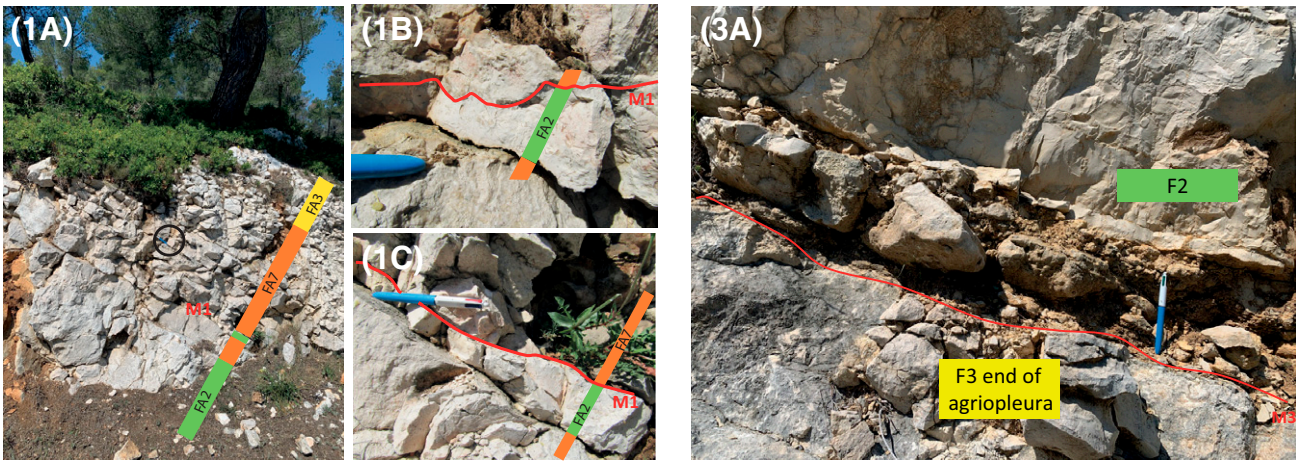


**Figure 10.** Outcrop pictures of negative accommodation events recorded in Martigues. (1A) General view of the M1 location (departmental road 5) with facies association interpretation. The black circle locates the pen, which is 10 cm in size. Refer to Figure 3 for facies legend. (1B, 1C) Close-up views of the irregular M1 surface, showing coarse-grained grainstone to rudstone (FA7) overlying a bird-eye mudstone (FA2). (3A) Top of the last Agriopleura-rich rudstone layer, capped by an irregular and brecciated surface composed of centimeter- to decimeter-sized angular to subangular clasts of rudist rudstone to grainstone within a reddish argillaceous matrix.

above which apparent accommodation consistently increases (Figure 10). At Mont Ventoux, the same evolution is observed, and M1 corresponds here to a firmground surface (Tendil et al., 2018). In southern Provence, the M1 marker is defined by an irregular stratigraphic surface showing subaerial exposure criteria. This surface separates two adjacent intervals formed in a positive accommodation context but defined by different bathymetry evolution and ΔB/T ratio. The cumulative apparent accommodation of the M0–M1 interval varies geographically with values increasing northward.

### M2 Marker

Whatever the geographic location, a change in the accommodation trend has been reported from the top of the upper Barremian *T. vandenheckii* ammonite subzone, defining the M2 marker. In southern Provence, M2 marks the culmination of an aggrading inner-platform interval (ΔB/T = 0) characterized by subaerial exposure evidence at Cassis (2 in Figure 1; Masse, 1976). From Orgon (5 in Figure 1) to Saint-Christol (16 in Figure 1; including Fontaine de Vaucluse), it is placed at the top of a shallowing upward interval (ΔB/T ratio < 0) and above which the accommodation pattern is increasing suddenly (ΔB/T > 0) (Figure 10). In northward sections such as at Banon (17 in Figure 1) and Mont-Ventoux (23 in Figure 1), the M2 marker would correspond to the top of a negative apparent accommodation event marked by a firmground surface (Tendil et al., 2018). The cumulative apparent accommodation of the M1–M2 interval reveals distinct patterns between southern Provence (+30 m) and northern Provence (from +130 to +198 m).

### M3 Marker

The M3 marker punctuates a stratigraphic interval characterized by several cycles of apparent accommodation across the study area. The M3 is identified at the top of the last negative apparent accommodation event (N7) (Figure 10). This event is associated with the development and major subaerial exposure of an inner platform from southern to northern Provence (Gorges de la Nesque section 20–22 in Figure 1) (Figures 9, 10). A drop of apparent accommodation ranging from −1.5 to −57 m and a bathymetric decrease from −10 to −65 m has been calculated. Above M3, apparent accommodation returns to positive and stable values over the whole study area.

### M4 Marker

The M4 marker is placed at the top of the aggrading inner-platform interval deposited in positive AAC context (ΔB/T = 0) and above which stand regional major changes of both lithostratigraphy and accommodation evolution (P9, Figure 10). Whatever the geographic location, a sharp apparent accommodation gain (ΔB/T > 0) is observed above M4: +90 to +130 m in southern and middle Provence, +10 to

+90 m in northern Provence (Figure 9). For the first time, apparent accommodation does not increase northward; an east–west trend is, rather, reported.

### M5 Marker

The M5 marker is supposed to date from the basal part of the upper Barremian *Martelites sarasini* ammonite subzone. It separates an underlying negative apparent accommodation interval (n8, $\Delta B/T < -1$) from an overlying positive one (Figure 9). The M4–M5 interval recorded a cumulated positive accommodation ranging from +4.5 to +81.5 m from northern Provence to southern Provence. In northern Provence, the eastern part still exhibits lower apparent accommodation values (+10 m) than the western part (+25 m).

### M6 Marker

The M6 marker has been identified in middle and northern Provence only where it represents the top of an aggrading inner platform formed in a positive accommodation pattern during the late Barremian (*M. sarasini* ammonite subzone). In northern Provence, it corresponds to a major stratigraphic surface (D2 sensu Masse et al., 2011), resulting from subaerial exposure and correlated at Banon and Mont-Ventoux with basinal an aggrading interval (17 and 23, respectively, in Figure 1).

### M7 Marker

The M7 marker is identified at the Banon and Mont-Ventoux sections (Figure 9), marking the top of a major negative apparent accommodation event (N9). This event is associated with the deposition of platform-derived facies associations (FA9) onto basinal facies (FA11/FA12). The estimated drop in apparent accommodation would range from −40 to −70 m. Above, apparent accommodation drastically increased again.

### M8 Marker

In northern Provence, a new increase of accommodation ($\Delta B/T > 0$) led to the drowning of the inner platform (P11 in Figures 7–12). But in the eastern part of northern Provence only, this new pulse of positive apparent accommodation dated here as early Aptian (base of *Deshayesites oglanlensis* ammonite subzone) is quickly followed by a negative AAC interval, whose top defines the M8 marker. The latter were identified from Font Jouvale to Banon sections (10 and 17 in Figure 1, respectively), which suggests a possible local tectonic event. Apparent accommodation from the M7–M8 interval ranges from 0 to +59 m and increases westward and northward from Oppedette, where no records have been observed (Figure 12).

### M9 Marker

A turnover of the apparent accommodation evolution has been reported at the top of early Aptian *D. oglanlensis* ammonite subzone (Tendil et al., 2018) from the stratigraphy in northern Provence. This change marks the M9 marker, which corresponds here to a hardground surface (Tendil et al., 2018). The M9 punctuates an interval defined either by a $\Delta B/T$ ratio = 0 or < 0 (i.e., Gorges de la Nesque) and above which a regional rise of apparent accommodation has been characterized (Figure 9). The apparent accommodation of the M7–M9 interval in northern Provence displays once again a positive trend westward. It may suggest the influence of an active fault system (such as the Salon-Cavaillon system fault) contributing to the progressive structuring of the western part of northern Provence and the deepening of the surrounding depositional areas (see further discussion).

### M10 Marker

Like the previous marker, the M10 marker corresponds to a hardground surface dated from the top of the lower Aptian *Deshayesites furcata* ammonite subzone (Tendil et al., 2018) in northern Provence. It separates an underlying interval consisting of outer-platform facies associations, deposited in a slightly positive AAC context with values ranging from +2 to +31 m. Above this interval, marly basinal facies dominate, indicating a significant increase in AAC values (Figure 9). The apparent accommodation calculated for the lower Aptian M9–M10 interval emphasizes high lateral variations in northern Provence. Here, apparent accommodations increase from +19 m at Oppedette to +31 m at Simiane la Rotonde (Figure 12), both sections being separated by only 4.5 km (13 and 14 in Figure 1). The same pattern is observed in the western part of northern Provence.

### M11 Marker

The M11 marker is dated from the top of the lower Aptian *D. furcata* ammonite subzone by Frau et al.

(2018) and has been recognized in several sections only due to post-Durancian erosion. It corresponds to the base of the global increase of apparent accommodation (+100 m) in northern Provence (Figure 9).

## INTERPRETATIONS AND DISCUSSIONS

### Stratigraphic Architectures of the Lower Barremian–Lower Aptian Carbonates in Provence

The definition of the stratigraphic architectures of the Urgonian system of Provence is based on the interpretation of the spatial and temporal evolutions of the apparent accommodation, ΔB/T ratio, facies proportions, and nature of stratigraphic surfaces. For each interval, a broad environmental trend followed by more detailed descriptions is given.

#### M0–M1 Stratigraphic Architectures

The first M0–M1 interval mainly characterizes an inner platform in southern Provence while bioclastic sand shoals developed in open marine influences until Orgon in middle Provence (Figure 11). Northward, slope facies associations and basin conditions developed (Figures 11, 12). The basal P1 positive accommodation event marks a southward retrogradation of the facies belts. The latter is subsequently followed by a general progradation phase interpreted from negative ΔB/T ratios. During the same time interval, aggradation of a restricted inner platform is inferred at Cassis (Figures 11, 12). Finally, the second prograding interval would be associated with the N3 major negative apparent accommodation event, which led to the decrease of the water depth and the subaerial exposure of the inner platform from southern Provence to Saint Chamas. Spatial facies evolution from southern to northern Provence indicates a ramp profile sensu Tucker and Wright (1990). The angle of this ramp could range from 0.02° to 0.10° from Cassis to Orgon and northward from Orgon, respectively.

#### M1–M2 Stratigraphic Architectures

Restricted inner-platform conditions extended from southern to middle Provence during the M1–M2 interval. Northward open marine influences still dominated, and bioclastic sand shoal complex developed until Saint Christol and Gorges de la Nesque in northern Provence (Figures 11, 12). This pattern results in the flattening of the ramp profile with mean angle ranging from 0.01° to 0.04°. No subaerial exposure criteria have been observed at the top of the interval. The bathymetric evolutions and ΔB/T ratios calculated at the base of the M1–M2 interval in northern Provence would suggest a possible diachronous sedimentation pattern compared to southern and middle Provence. The first pulse of accommodation only recorded in northern Provence results in the development of margin and slope environments extending to middle Provence, while southern Provence remained exposed (Figures 11, 12). Onlapping geometries would be expected from bathymetric and accommodation patterns only. The uppermost part of the M1–M2 unit is characterized by a positive accommodation pattern recorded throughout the study area. The ΔB/T ratio = 0 in southern Provence still points to the aggradation of the inner platform. The ΔB/T ratios < 0 in middle Provence and northern Provence emphasize the efficiency of the carbonate production factory to fill the created available space during deposition of the M1–M2 unit (Figures 11, 12).

#### M2–M3 Stratigraphic Architectures

The M2–M3 interval is characterized by the continued development of inner-platform environments in southern and middle Provence, while open marine conditions prevailed in northern Provence. Slope environments in the northernmost sections, such as Mont-Ventoux and Banon, transition into basinal settings (Figures 11, 12). As described in the Apparent Accommodation Calculation and Marker Identification section, this interval is marked by three to four cycles of positive and negative apparent accommodation. In northern Provence, four distinct cycles, with thicknesses ranging from 15 to 100 m, have been identified. These cycles reflect ~10-km-scale retrogradations and progradations of facies belts, inferred from the alternations between slope and outer-platform environments (Figures 11, 12). In contrast, in southern Provence, three cycles of apparent accommodation are recorded, with facies alternations between inner-platform and outer-platform environments over accumulations of 15–25 m.

The second cycle within this interval exhibits maximum retrogradation of facies belts, corresponding

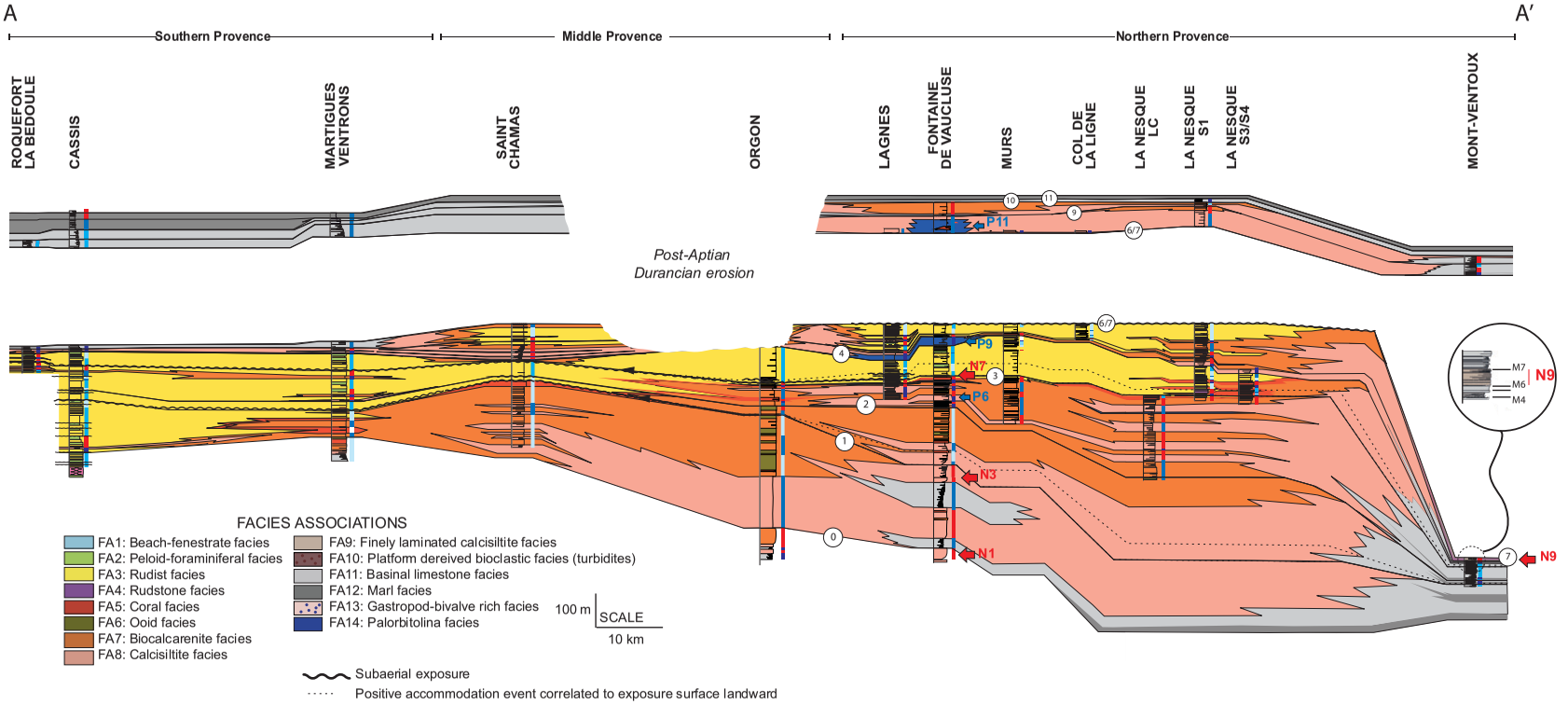


**Figure 11.** Stratigraphic architectures from southern Provence to the western part of the northern Provence. Wavy bold lines correspond to emersion surfaces inferred from either geological field observations or from apparent accommodation pattern (top of a negative apparent accommodation event). Dashed lines correspond to positive accommodation interval locally recorded correlated to exposure surface landward suggesting onlapping stratal geometries. See Figure 1 for location of the cross section. Uppercase = major event; lowercase = minor event. LA NESQUE LC = Gorge de la Nesque Le Cire; LA NESQUE S1 = Gorge de la Nesque Section 1; LA NESQUE S3/S4 = Gorge de la Nesque Section 3/Section 4 (see Léonide et al, 2012); N = negative accommodation event; P = positive accommodation event.

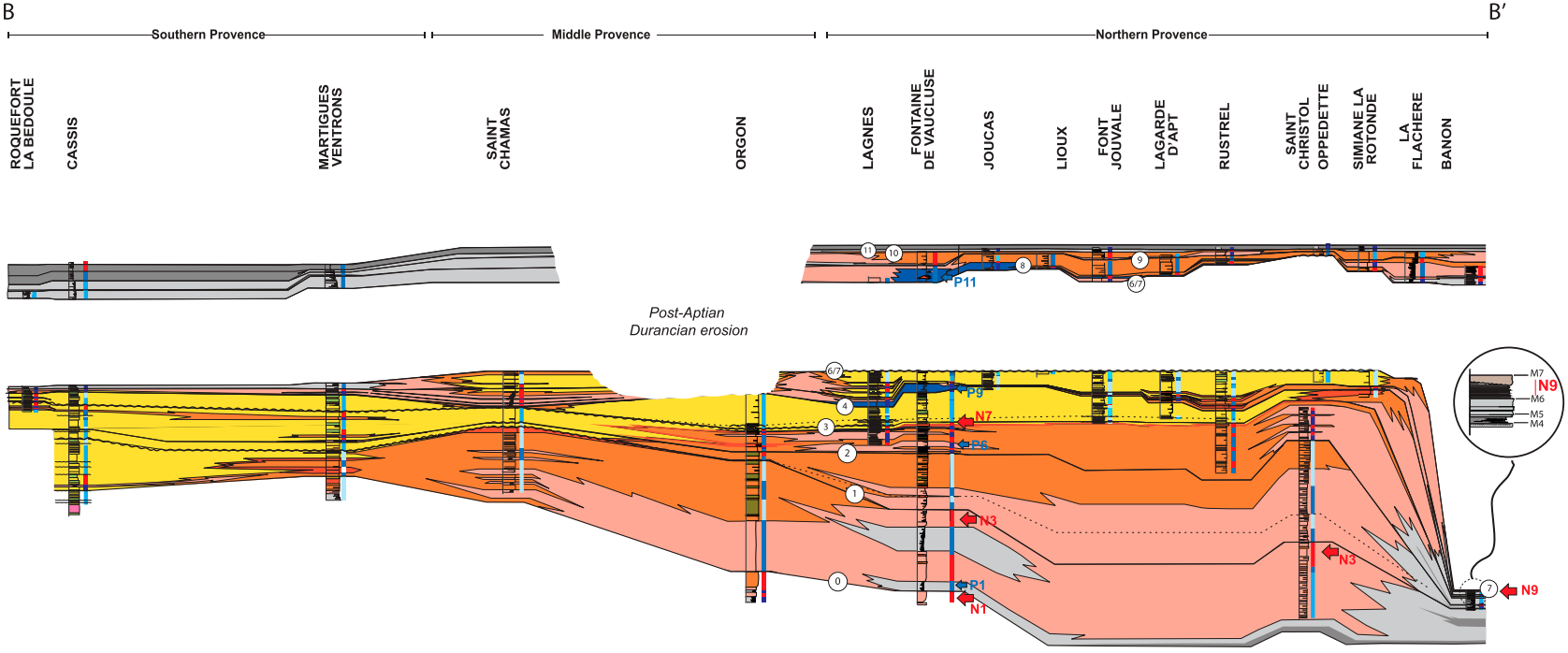


**Figure 12.** Stratigraphic architectures from southern Provence to the eastern part of northern Provence. Wavy bold lines correspond to exposure surfaces inferred from either geological field observations or from apparent accommodation pattern (top of a negative apparent accommodation event). Dashed lines correspond to positive accommodation intervals locally recorded correlated to emersion surface landward suggesting onlapping stratal geometries. See Figure 1 for location of the cross section. Uppercase = major event; lowercase = minor event. N = negative accommodation event; P = positive accommodation event.

to a general bathymetric increase. This retrogradation is evidenced in both southern and northern Provence. The uppermost N7 negative apparent accommodation episode recorded in most of the sections from the study area results in (1) a drastic seaward migration of the facies belts, (2) the overall extension of inner-platform environments from southern to northern Provence, and (3) a regional subaerial exposure till the Gorges de la Nesque and Rustrel sections. In southern Provence, this episode is coeval with the last occurrence of Agriopleura rudist fauna.

### M3–M4 Stratigraphic Architectures

In middle and northern Provence, the base of the M3–M4 interval, formed in a positive apparent accommodation framework, is marked by the accumulation of Agriopleura-rich rudist facies (FA3). In southern Provence, the latter rudist fauna disappeared with the underlying negative apparent accommodation event and exposure of the platform. This consequently reflects the development of an inner platform from middle Provence to northern Provence onlapping the subaerially exposed southern Provence (Figures 11, 12). As apparent accommodation continues to increase, inner-platform environments developed from southern to northern Provence, indicating a very flat topography over more than 120 km with some structural irregularities such as at Saint-Chamas. The inner platform was protected from the high hydrodynamic open-marine conditions by an ~3-km-wide coral complex at the Gorges de la Nesque section and at the Simiane la Rotonde section eastward (20–22 and 14 in Figure 1; Figures 11, 12). Finally, lower hydrodynamic open-marine environments are recorded northward. No subaerial exposure criteria have been observed at the top of the interval, except some local beach-rocks (FA1) at Gorges de la Nesque section (Léonide et al., 2012).

### M4–M5 Stratigraphic Architectures

The regionally observed positive P9 event points to the drowning of the underlying inner platform, but the latter has been differently expressed, depending on the geographic position. In northern Provence, high hydrodynamic shallow outer platform to slope environments developed in its eastern and western parts, respectively. The first Palorbitolina unit is deposited in the western part of northern Provence exclusively. Basin environments still characterize northern sections from Banon and Mont-Ventoux (Figures 11, 12). In southern Provence, a higher pulse of apparent accommodation than northward boosts the development of slope to basin conditions. Consequently, at this time, the shallowest environments are restricted to an isolated zone located in the eastern part of northern Provence. The overlying n8 negative apparent accommodation event is associated with the decrease of water depths and the return of shallow subtidal inner-platform conditions in only northern Provence, while the southern Provence remains under basin settings.

### M5–M6 Stratigraphic Architectures

In northern Provence, this interval is characterized by the aggradation of inner-platform environments. No coral complex has been observed on the platform margin to protect the inner restricted realm as for the underlying intervals. Besides, the accumulation of coral gravel and coarse rudist facies associations indicates a higher hydrodynamic inner platform than in previous intervals. These environments extended until La Flachère and Gorges de la Nesque (15 and 20 in Figure 1) through 10- to 15-km northward progradation, which rapidly evolved to the outer platform and basin conditions. Similarly, a 5- to 10-km southward progradation of the inner-platform environments is inferred at Rustrel and Lagnes. Consequently, the M5–M6 interval characterizes the general development of the northern Provence isolated carbonate platform, on either side of which slope and basin environments developed in less than ~10 km, suggesting high slope angle from 0.4° to 1.15°. The top of this interval exhibits a very sharp planar surface to irregular epikarstic surface interpreted by Tendil et al. (2018) as emersion surface. A second high-hydrodynamic inner carbonate platform is recorded at Saint-Chamas (4 in Figure 1) in middle Provence, while southern Provence remains under the influence of deep basin conditions. Recent erosion and lack of lateral continuity of outcrops prevent knowing if such environments developed until Orgon (5 in Figure 1) and if lateral connectivity between this platform and the northern Provence inner platform exists.

### M6–M7 Stratigraphic Architectures

The major N7 negative apparent accommodation event ($\Delta B/T < -1$) during the M6–M7 interval caused a significant decrease in water depth, resulting in the development of slope environments that replaced the deeper conditions in the northernmost part of the platform (Figures 10, 11). During this interval, the supposed subaerial exposure of the northern Provence inner platform thus evolved to slope environments in less than 10 km, suggesting slope angle from 0.2° to 1.0°. Basin conditions still prevailed in middle and southern Provence.

### M7–M8 Stratigraphic Architectures

This interval, dated to the Barremian–Aptian transition, characterizes an apparent accommodation cycle recorded only in the eastern part of northern Provence. The base of the cycle marks the drowning of the previously exposed inner carbonate platform in northern Provence, while southern and middle Provence remained influenced by basin conditions (Figures 10, 11). The post-Aptian Durancian erosion does not allow for study of the relationships between the middle to southern Provence areas. The westward increase of apparent accommodation from Oppedette (13 in Figure 1), associated with the progressive deepening of depositional environments, points to a structuring of the sedimentary profile, evolving to a 60-km-wide gentle slope from Oppedette toward Fontaine de Vaucluse and Lagnes sections (Figure 12). A similar environmental evolution is described from Oppedette toward Banon northward in only 7 km, suggesting a more abrupt ramp profile. The M7–M8 would thus highlight possible structural influences on the sedimentation pattern.

### M8–M9 Stratigraphic Architectures

Although the M8–M9 interval is characterized by an aggrading trend in the western part of northern Provence, a different pattern is observed in its eastern part. Indeed, bioclastic sand shoals finally covered the previous exposed Oppedette area (13 in Figure 1). These conditions extended to Banon at the top of the interval, resulting from an uppermost negative apparent accommodation event locally recorded ($\Delta B/T$ ratio $< -1$). This points once again to the activity of fault systems, which would have led to the uplift of the Banon area and the appearance of shallower and higher hydrodynamic conditions northward (Figure 12). The top of this interval is marked by a hardground regionally observed (Tendil et al., 2018). In southern and middle Provence, deep and low energy basin to slope environments still dominated.

### M9–M10 Stratigraphic Architectures

The M9–M10 interval characterizes the broad extension of a high hydrodynamic outer-platform environment across northern Provence surrounded by slope and basin environments both to the southern and northward from the Gorges de la Nesque area. In more detail, it appears that kilometer-wide areas upon which only outer-platform environments developed (such as at Joucas and Oppedette) are separated by deeper zones where slope environments prevailed (Figures 11, 12). The progradation of bioclastic sand shoal into these depressions led to the decrease of water depth and the general extension of outer-platform conditions. The development of the deeper depositional conditions coincides with the geographic distribution of the highest apparent accommodation values and $\Delta B/T$ ratio $> 0$ at the base of the interval, suggesting the impact of local fault activity. According to Kandel (1992), kilometer-wide half graben systems may have been created throughout northern Provence in the early Aptian, affecting the distribution of the depositional environments.

### M10–M11 Stratigraphic Architectures

The M10–M11 interval, dated from the lower Aptian *Deshayesites forbesi* ammonite subzone, characterizes an overall increase of apparent accommodation (+100 m), associated with the widespread development of basin conditions from southern to northern Provence.

## Controlling Factors of Stratigraphic Architectures

Stratigraphic architecture of the Urgonian platform is interpreted with respect to the paleoclimatic, oceanographic, eustatic, and tectonic evolution in the Early Cretaceous.

### Carbonate Production and Climatic Conditions

The Barremian and early Aptian are commonly considered greenhouse periods, with the study area located approximately 28–30°N from the paleoequator,

creating favorable conditions for intense carbonate accumulation on the southern margin of the Vocontian Basin.

During the Hauterivian to early Barremian, mesotrophic to eutrophic conditions, inferred from high nutrient levels and a humid climate (Godet et al., 2006; Huck et al., 2011, 2013), may have (1) limited the development of photosynthetic organisms and (2) restricted inner platform growth to southern Provence during the M0–M1 interval. The mid-Barremian event affected the western Tethys at the end of the early Barremian (Mutterlose et al., 2009; Huck et al., 2011, 2013), but its impact is not clearly visible in the stratigraphy of southern and northern Provence.

From the late Barremian (*T. vandehenckii* to *I. giraudi* ammonite subzones), bioclastic sand shoal complexes developed widely (M1–M2 interval), followed by the expansion of inner-platform environments into northern Provence (M2–M4 interval). This environmental change, the extensive growth of photozoan organisms (e.g., rudists and green algae), and the evolution from a ramp to a carbonate platform suggest increased carbonate production, probably influenced by a return to a colder, arid climate (Bodin et al., 2009; Mutterlose et al., 2009). The M4–M5 interval (upper Barremian *I. Giraudi* subzone) records the decline of photozoan organisms (Mutti and Hallock, 2003) and a resurgence of heterozoan groups, likely due to mesotrophic to eutrophic conditions associated with the warmer, short-lived, humid Taxy event, which led to higher nutrient levels and organic-rich layers in the western Tethys (Huck et al., 2011, 2013). The end of the late Barremian was characterized by a return to oligotrophic conditions, fostering the growth of a carbonate platform in northern Provence. This pattern, also observed in the Jura and Helvetic regions, would be concomitant with the global return to arid and cold conditions (Bodin et al., 2009; Mutterlose et al., 2009).

The early Aptian was marked by extreme temperature increases, eutrophic conditions, humidity, and rising volcanic activity. In northern Provence, the drowning of the late Barremian inner platform and the expansion of outer-platform environments dominated by heterozoan organisms during the M6–M9 interval indicate the return of mesotrophic conditions and deteriorating climatic and environmental conditions. The final drowning of the northern Provence outer platform during the M10–M11 interval indicates a decrease in carbonate production, coinciding with the OAE1a (Erba et al., 2015).

### Eustatic Fluctuations

Stratigraphic architectures can be good indicators of eustatic variations under particular geodynamic conditions. In a nonsubsiding area, sea-level falls can result in a seaward migration of the facies belt by sedimentary progradations and a common (but not systematic) subaerial exposure of the inner part of the sedimentary profile. On the contrary, sea-level rises can be associated with the progressive deepening of the water depths if sediment supply is lower than the accommodation, which results in a landward migration of the facies belt and a retrogradation. The quantitative sequence stratigraphic approach (Borgomano et al., 2020) can help to reconstruct the eustatic sea-level changes that are discussed in the following paragraphs.

The consistency of the eustatic curve from Haq (2014) is discussed according to the apparent accommodation and stratigraphic architectures of Barremian to lower Aptian sequences. Four regional negative and positive apparent accommodation events associated with progradational and retrogradational patterns, respectively, have been identified in the Urgonian carbonates of Provence (until the *Deshayesites deshayesi* ammonite subzone). During the same time interval, Haq (2014) reported four third-order eustatic cycles, each of them lasting approximately 1.4 to 1.7 m.y.

The first negative event of apparent accommodation (below the M0 marker) in the early Barremian would be time-equivalent to the worldwide drastic eustatic fall (–95 m) dated at 130.4 Ma by Haq (2014) (Figure 13). In Provence, the apparent accommodation was approximately −50 m for M0, suggesting that sea-level fall would have been compensated by regional subsidence. Following M0, a regional increase in apparent accommodation and facies retrogradation occurred during the early Barremian (*Nicklesia nicklesi* to *N. pulchella* ammonite zones; 130.4 to 129.7 Ma; *Emericiceras* sp. ammonite found in Fontaine de Vaucluse section by Masse, 1976). This event aligns with the sea-level rise reported by Haq (2014) in the early Barremian,

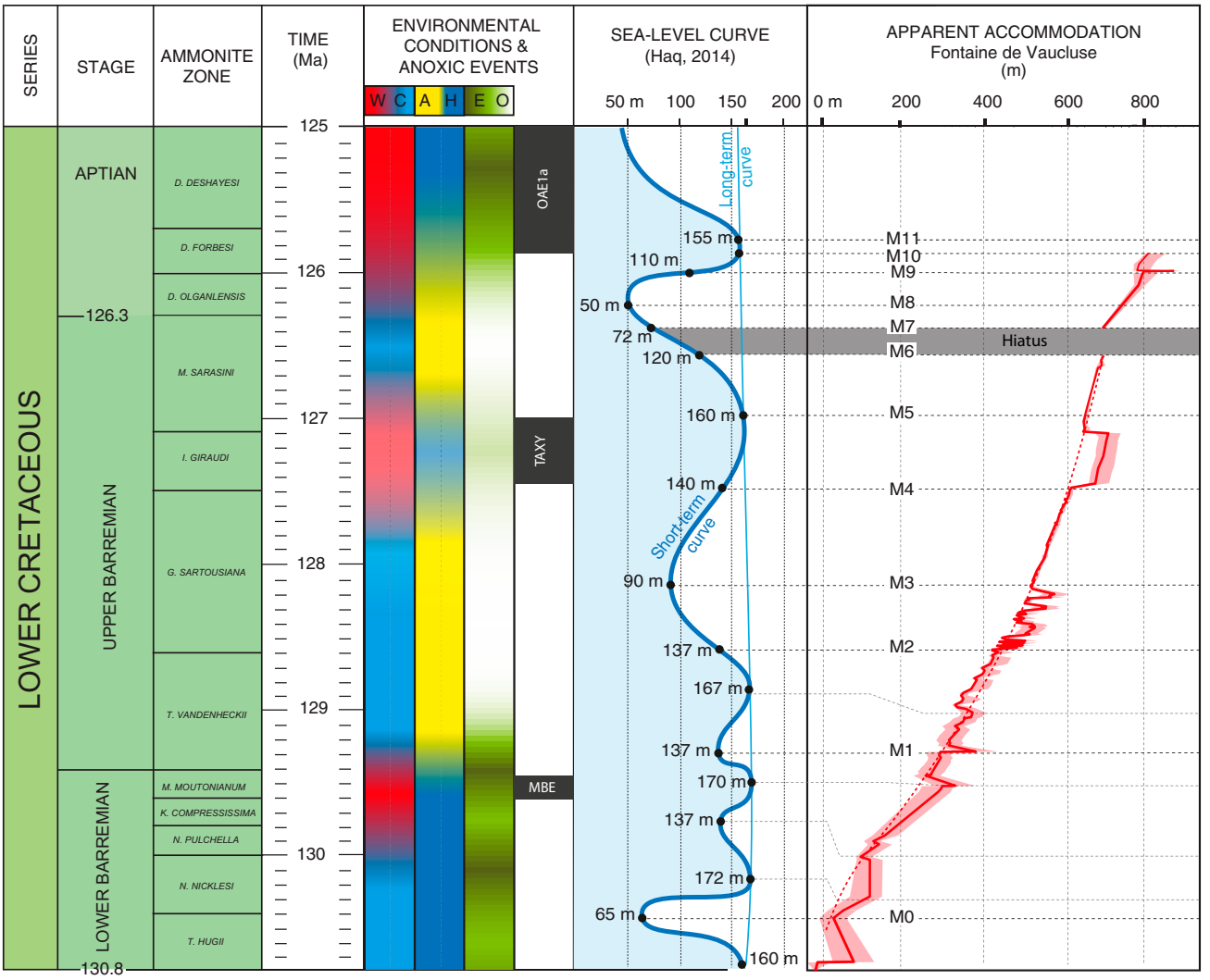


**Figure 13.** Sea-level apparent accommodation evolution at Fontaine de Vaucluse as a function of sea-level changes (Haq, 2014), environmental conditions, and anoxic events (Bodin et al., 2006; Godet et al., 2006; Mutterlose et al., 2009; Huck et al., 2011, 2013) from early Barremian to early Aptian. Accommodation markers are dated resulting from biostratigraphic constraints. Uncertainties related to this dating would range from 0.2 to 0.4 m.y. A = arid; C = cold; E = eutrophic; H = humid; MBE = mid-Barremian event; O = oligotrophic; OAE = ocean anoxic event; TAXY = Taxy event; W = warm.

associated with a +110-m rise. The latter, however, is lower than the apparent accommodation reported in middle and northern Provence (+250 to +360 m), suggesting once again regional subsidence influences.

A subsequent worldwide eustatic drop was reported by Haq (2014) before the M1 geochron at the base of the upper Barremian. However, criteria such as the northward facies progradation, decreasing water depths, and inner-platform subaerial exposure in southern Provence suggest an accommodation space reduction, related to eustacy and/or tectonics. As the M1 marker separates two adjacent units deposited under different climatic and environmental conditions, whose transition is dated from the top of the *Moutoniceras moutonianum* and *Paraceratites elegans* ammonite subzones in the Tethyan and Boreal regions, respectively (McArthur et al., 2004), M1 would be consequently coeval with the end of the eustatic fall reported by Haq (2014). Nonetheless, the fact that no such event would be recognized in the adjacent Tethyan realm (Frau et al., 2020) suggests either a limited fall of sea level and/or a sea-level fall greatly compensated by an important regional subsidence. Indeed, the high variability of interval thickness of the sections points also to an important differential subsidence effect.

In the study area, a second major positive accommodation event recognized at the base of the M2–M3 interval is associated with general bathymetric deepening and a regional retrogradation of facies belts. No climatic or environmental changes are reported to explain this evolution. The creation of accommodation space by a rise in sea level may be a possibility. Nevertheless, no eustatic rise has been reported on the reference Cretaceous curve during the late Barremian (*G. sartousiana* ammonite zone). Indeed, the eustatic rise reported by Haq (2014) would end earlier in the late Barremian (*T. vandenheckii* ammonite zone) (Figure 13). It would thus be naturally associated with the deposition of the underlying M1–M2 interval. Other processes such as tectonic activity might have influenced the accommodation pattern during the M2–M3 interval in Provence, leading to a regional increase of apparent accommodation.

The sudden seaward migration and subaerial exposure of inner-platform environments at the top of the M2–M3 interval indicate a regional drop in apparent accommodation ($\Delta B/T$ ratio $< -1$). This event, dated to the late Barremian (*G. sartousiana* ammonite zone), aligns with time-equivalent observations in adjacent Tethyan realms (Bas-Vivarais, Switzerland, Spain; Frau et al., 2020) and may point to a global fall in sea level. Haq (2014) reported such a worldwide eustatic fall at the beginning of the late Barremian, which can thus be considered to have also impacted southern France (Figure 13).

The drastic regional increase of apparent accommodation during the M4–M5 interval, leading to the drowning of the underlying inner platform and the reappearance of deeper depositional environments from southern to northern Provence can be interpreted in different ways. On the one hand, the return of climatic-driven mesotrophic conditions may have contributed to weakening the activity of carbonate factory, limiting the carbonate accumulations, and favoring the increase of water depths. Nevertheless, according to Haq (2014), a sea-level rise phase ended during the late Barremian *I. giraudi* ammonite subzone (Figure 13). Therefore, continuous carbonate production of the inner platform (M3–M4 interval) likely initially counteracted the sea-level rise, maintaining a relatively stable water depth and promoting aggradation. However, the subsequent drowning of the latter may thus reflect the cumulative effect of the eustatic rising and the weakening activity of the carbonate factory due to the mesotrophic climatic conditions. Finally, considering the nonuniform geographic distribution of the apparent accommodation from northern Provence to southern Provence and from east to west in northern Provence, tectonic influence may have contributed to the stratigraphic architectures during the upper Barremian M4–M5 interval.

During the late Barremian, the return to arid and cold climatic conditions led to the reappearance of photozoan organisms in the M5–M7 interval in northern Provence. These accumulations are marked by regional stratigraphic surfaces likely due to subaerial exposure (Tendil et al., 2018). Similar criteria observed in other Mediterranean Tethys platforms (Frau et al., 2020) suggest a global eustatic fall at the end of the Barremian, as reported by Haq (2014). In northern Provence, subaerial exposure of the inner platform coincided with a negative apparent accommodation event in basin sections (e.g., Banon, Mont-Ventoux). Borgomano et al. (2020) noted that proximal records are incomplete due to exposures and hiatuses, whereas distal sections preserve the complete accommodation signal. This supports the hypothesis of a global eustatic fall at the end of the Barremian (Haq, 2014). Conversely, the positive apparent accommodation in southern Provence indicates local structural processes causing high subsidence.

At the beginning of the early Aptian, the inner exposed platform in northern Provence drowned. The basal retrogradation of facies belts and increased apparent accommodation could have been induced by a eustatic rise, such as the one reported by Haq (2014) at the base of the lower Aptian, which would apparently be slightly postponed related to the drowning of the inner platform. Furthermore, except in Spain, where basin conditions developed onto the underlying inner exposed platforms, synsedimentary hiatus occurred in other platforms from the Mediterranean Tethys (Frau et al., 2020), pointing probably to a limited eustatic influence. Besides, the westward and northward nonuniform increase of apparent accommodation from the Oppedette area and the creation of kilometer-scale depocenters and topographic highs suggest a structuring of the depositional area

by active fault systems. Whatever the eustatic and/or tectonic origins, drowning is coeval with the worldwide degradation of the climatic and environmental conditions, which marks the return of mesotrophic conditions. Such conditions could have weakened the activity of carbonate factory, contributing to limit the carbonate accumulation and consequently to increase the water depths. Finally, the M10–M11 interval is characterized by a general increase of apparent accommodation, and the development of deeper basin conditions may result from the cumulative effect of the sea-level rise reported on the Cretaceous reference curve (Haq 2014) during the OAE1a.

## Interest of the Method

Carbonate sequence stratigraphic models typically assume that a single A/S signal represents the entire stratigraphic architecture, allowing correlation throughout the carbonate system. However, this assumption frequently overlooks the variability in accommodation and sediment supply over time. Additionally, A/S ratio changes are commonly interpreted as sea-level changes (Sharland et al., 2001), but such models are rarely validated through quantitative forward modeling.

The first point is the fact that this method offers the opportunity for challenging the interpretation of the facies association, their relationships, and, finally, the evolution of the deposition environment (i.e., water depth). Although this study uses water depths from previous research, they can also be inferred from sedimentological interpretations of facies. Incorporating uncertainty in water depths allows for the construction of multiple accommodation scenarios, which can be tested, validated, or adjusted using stratigraphic forward modeling tools. Unlike the assumption of uniform eustatic variations, focusing on accommodation reveals interactions with other factors, such as subsidence patterns, which can vary geographically. Consequently, considering a reference eustatic curve for a given time interval, it is possible to quantify the influence of the apparent accommodation resulting from differential subsidence in every location of a sedimentary basin.

The second point is that we have demonstrated that an explicit method is possible. Apparent accommodation curves can be constructed for all locations within a carbonate system using measurable data from outcrops or cores. A high-resolution stratigraphic framework can then be developed through (1) lateral correlation of apparent accommodation trends and $\Delta B/T$ ratios, and (2) interpretation of major stratigraphic surfaces (exposure or drowning surfaces). However, without a well-constrained chronostratigraphic framework, these correlations can lead to inconsistencies and diachronic issues. For example, correlating negative accommodation events from the inner platform to the outer shelf can be complex, but with accurate chronostratigraphic data, we can align inner-platform exposures ($\Delta B/T$ ratios $-1$ to 0) with outer-platform and outer-shelf negative accommodations ($\Delta B/T$ ratio $< -1$). In the inner platform, because of exposures and stratigraphic hiatuses, apparent accommodation does not match the real accommodation systematically, whereas the record of the latter is more continuous in the deeper environments due to higher accommodation space.

This method has improved the characterization of stratigraphic geometries in the studied area, identifying lowstand intervals in northern Provence, while southern Provence remained subaerially exposed. By analyzing accommodation below and above major stratigraphic surfaces, we achieve a more robust interpretation of stratigraphic architecture.

Nevertheless, this method has limitations. It relies heavily on prior estimation of facies depositional environments. Sharp changes in apparent accommodation smaller than paleo water depth ranges may not be detected. A well-constrained chronostratigraphic framework is also essential for accurate time-thickness functions and carbonate production rates. Without it, accommodation markers may intersect real chronostratigraphic timelines, distorting reservoir architectures. For subsurface data with uncertain chronostratigraphy, we suggest multiple scenarios of accommodation and sedimentation rates tested using stratigraphic forward modeling tools.

Finally, the method's suitability depends on the sedimentary system and case study. It is most effective when significant spatial and temporal variations in thickness and facies water-depth exist. Even in cases with uniform water depth, such as Middle Eastern carbonate reservoirs, spatial thickness variations can still reveal accommodation changes. These variations, influenced by local tectonics, can be quantified and tested through stratigraphic forward modeling.

## CONCLUSIONS

When seismic images or continuous outcrops are unavailable, constructing three-dimensional (3-D) stratigraphic architectures of carbonate platforms typically relies on standard sequence stratigraphic correlations. However, this method, despite its common use, is implicit, qualitative, and based on strong assumptions.

This study introduces a novel approach to establish the stratigraphic architectures applied to the Barremian–lower Aptian Urgonian carbonate platform in Provence. It uses a recently published quantitative method that integrates the correlation of apparent accommodation trends across distant locations and introduces a new parameter: the ΔB/T ratio. Unlike the traditional A/S ratio, the ΔB/T ratio is directly measurable and enhances understanding of the processes governing the formation of specific stratigraphic intervals and their correlation.

Four successive major negative apparent accommodation events were identified, predominantly in outer-shelf domains, and were correlated with subaerially exposed units in shallower inner environments. Positive accommodation events were easier to correlate, as they were consistently recorded across all locations of the carbonate sedimentary system.

This new high-resolution quantified stratigraphic framework reveals a morphologic evolution of carbonate platform during the early Barremian to the beginning of the late Barremian. It highlights the cumulative influence of carbonate production and negative apparent accommodation events, driving multiple seaward progradations of the facies belt. Spatial variability in the cumulative apparent accommodation suggests significant tectonic influences on platform evolution. The end of the late Barremian was marked by an inversion of the accommodation polarity toward southern Provence, pointing to geodynamic structuring of the study area. In the early Aptian, successive accommodation pulses and a climatic factor would have led to the progressive drowning of the platform.

In conclusion, the method of quantitative sequence stratigraphy and the introduction of the ΔB/T ratio represent an interesting advancement. They provide an explicit and nuanced understanding of the sedimentological processes driving stratigraphic evolution. This method not only facilitates robust sedimentological interpretations, but also allows for the formulation of multiple geological scenarios of accommodation evolution and needs to then be tested using 3-D forward sedimentological reservoir simulations.

When seismic data or continuous outcrops are unavailable, constructing 3-D stratigraphic architectures of carbonate platforms frequently relies on standard sequence stratigraphic correlations. Although widely used, this traditional method is largely qualitative, implicit, and based on strong assumptions, which can limit its predictive capabilities.

This study introduces a quantitative approach to define stratigraphic architectures, applied to the Barremian–lower Aptian Urgonian carbonate platform in Provence. The approach integrates apparent accommodation trends across geographically distant locations with a new parameter, the ΔB/T ratio. Unlike the traditional A/S ratio, which is inferred indirectly, the ΔB/T ratio is directly measurable and provides additional insights into the processes driving the formation and correlation of specific stratigraphic intervals.

Four successive major negative apparent accommodation events were identified, predominantly in outer-platform environments, and were correlated with subaerial exposure surfaces in shallower inner-platform settings. In contrast, positive apparent accommodation events were consistently recorded across all locations, making them easier to correlate.

The results reveal a detailed morphologic evolution of the carbonate platform from the early Barremian to the beginning of the late Barremian. The platform evolved through multiple seaward progradations of facies belts, driven by the combined influence of carbonate production and episodic negative apparent accommodation events. Spatial variability in cumulative apparent accommodation highlights significant tectonic controls on platform evolution. By the end of the late Barremian, a shift in accommodation polarity toward southern Provence indicates regional geodynamic restructuring. During the early Aptian, successive accommodation pulses, coupled with climatic influences, likely drove the progressive drowning of the platform.

The method of quantitative sequence stratigraphy, combined with the ΔB/T ratio, represents a significant advancement in understanding carbonate platform dynamics. This approach provides a nuanced, explicit interpretation of the sedimentological processes governing stratigraphic evolution.

Furthermore, it enables the construction of robust geological scenarios for accommodation evolution, which can be validated and refined through 3-D forward sedimentological and reservoir simulations.

## REFERENCES CITED


Arnaud, H., A. Arnaud-Vanneau, M. C. Blanc-Alétru, T. Adatte, M. Argot, G. Delanoy, J.-P. Thieuloy, et al., 1998, Répartition stratigraphique des orbitolinidés de la plate-forme urgonienne subalpine et jurassienne (SE de la France): Géologie Alpine, v. 74, p. 3–89.

Bastide, F., 2014, Synthèse de l'évolution de la plateforme Urgonienne (Barrémien tardif a aptien précoce) du Sud-Est de la France: Faciès, micropaléontologie, géochimie, géométries, paléotectonique et géomodélisation: Grenoble, France, Université de Grenoble, 300 p.

Bodin, S., N. Fiet, A. Godet, V. Matera, S. Westermann, A. Clément, N. M. M. Janssen, P. Stille, and K. B. Föllmi, 2009, Early Cretaceous (late Berriasian to early Aptian) palaeoceanographic change along the northwestern Tethyan margin (Vocontian Trough, southeastern France): $\delta^{13}C$, $\delta^{18}O$ and Sr-isotope belemnite and whole-rock records, Cretaceous Research, v. 30, no. 5, p. 1247–1262, doi:10.1016/j.cretres.2009.06.006.

Borgomano, J., C. Lanteaume, P. Léonide, F. Fournier, L. F. Montaggioni, and J. P. Masse, 2020, Quantitative carbonate sequence stratigraphy: Insights from stratigraphic forward models: AAPG Bulletin, v. 104, no. 5, p. 1115–1142, doi:10.1306/11111917396.

Borgomano, J., J. P. Masse, and S. Al Maskiry, 2002, The lower Aptian Shuaiba carbonate outcrops in Jebel Akhdar, northern Oman: Impact on static modeling for Shuaiba petroleum reservoirs: AAPG Bulletin, v. 86, no. 9, p. 1513–1529, doi:10.1306/61EEDCE2-173E-11D7-8645000102C1865D.

Bover-Arnal, T., H. Löser, J. A. Moreno-Bedmar, R. Salas, and A. Strasser, 2012, Corals on the slope (Aptian, Maestrat Basin, Spain): Cretaceous Research, v. 37, p. 43–64, doi:10.1016/j.cretres.2012.03.001.

Burla, S., U. Heimhofer, P. A. Hochuli, H. Weissert, and P. W. Skelton, 2008, Changes in sedimentary patterns of coastal and deep-sea successions from the North Atlantic (Portugal) linked to early Cretaceous environmental change: Palaeogeography, Palaeoclimatology, Palaeoecology, v. 257, no. 1–2, p. 38–57, doi:10.1016/j.palaeo.2007.09.010.

Catuneanu, O., W. E. Galloway, C. G. S. C. Kendall, A. D. Miall, H. W. Posamentier, A. Strasser, and M. E. Tucker, 2011, Sequence stratigraphy: Methodology and nomenclature: Newsletters on Stratigraphy, v. 44, no. 3, p. 173–245, doi:10.1127/0078-0421/2011/0011.

d'Orbigny, A., 1850, Prodrome de Paléontologie stratigraphique universelle des animaux mollusques et rayonnés: Masson, Paris, v. 1, 394 p.

Droste, H., 2010, High-resolution seismic stratigraphy of the Shu'aiba and Natih formations in the Sultanate of Oman: Implications for Cretaceous epeiric carbonate platform systems, *in* F. S. P. van Buchem, K. D. Gerdes, and M. Esteban, eds., Mesozoic and Cenozoic carbonate systems of the Mediterranean and the Middle East: Stratigraphic and diagenetic reference models: Geological Society, London, Special Publications 2010, v. 329, p. 145–162, doi:10.1144/SP329.7.

Eberli, G. P., C. Betzler, and F. Anselmetti, 2004, Carbonate platform to basin transitions on seismic data and in outcrops: Great Bahama Bank and the Maiella Platform Margin, Italy, *in* G. P. Eberli, J. L. Masaferro, and J. F. Sarg, eds., Seismic imaging of carbonate reservoirs and systems: AAPG Memoir 81, p. 207–250.

Erba, E., R. A. Duncan, C. Bottini, D. Tiraboschi, H. Weissert, H. C. Jenkyns, and A. Malinverno, 2015, Environmental consequences of Ontong Java Plateau and Kerguelen Plateau volcanism: Geological Society of America Special Paper, v. 511, 33 p., doi:10.1130/2015.2511(15).

Espurt, N., J. C. Hippolyte, M. Saillard, and O. Bellier, 2012, Geometry and kinematic evolution of a long-living foreland structure inferred from field data and cross section balancing, the Sainte-Victoire system, Provence, France: Tectonics, v. 31, no. 4, TC4021, 27 p., doi:10.1029/2011TC002988.

Fenerci-Masse, M., J. P. Masse, and E. Pernarcic, 2005, Quantitative stratigraphy of rudist limestones and its bearing on spatial organisation of rudist communities: The Late Barremian, Urgonian, sequences of Provence (S.E. France): Palaeogeography, Palaeoclimatology, Palaeoecology, v. 215, no. 3–4, p. 265–284, doi:10.1016/j.palaeo.2004.09.008.

Frau, C., G. Delanoy, and E. Hourqueig, 2015, Le genre Macroscaphites Meek, 1876 (Ammonoidea, dans l'Aptien inférieur de Cassis-La Bédoule (Bouches-du-Rhône, France. Proposition d'un nouveau schéma zonal pour la série stratotypique: Revue de Paléobiologie, v. 34, p. 45–57, doi:10.5281/zenodo.18899.

Frau, C., A. J.-B. Tendil, C. Lanteaume, J.-P. Masse, A. Pictet, L. G. Bulot, T. Luber, et al., 2018, Late Barremian/early Aptian ammonite bioevents from the Urgonian-type series of Provence (southeast France): Regional stratigraphic correlations and implications for the peri-Vocontian carbonate platforms: Cretaceous Research, v. 90, p. 222–253, doi:10.1016/j.cretres.2018.04.008.

Frau, C., A. J.-B. Tendil, A. Pohl, and C. Lanteaume, 2020, Revising the timing and causes of the Urgonian rudistid-platform demise in the Mediterranean Tethys: Global and Planetary Change, v. 187, 103124, 12 p., doi:10.1016/j.gloplacha.2020.103124.

Godet, A., S. Bodin, K. Follmi, J. Vermeulen, S. Gardin, N. Fiet, T. Adatte, Z. Berner, D. Stuben, and B. Vandeschootbrugge, 2006, Evolution of the marine stable carbon-isotope record during the early Cretaceous: A focus on the late Hauterivian and Barremian in the Tethyan realm: Earth and Planetary Science Letters, v. 242, no. 3–4, p. 254–271, doi:10.1016/j.epsl.2005.12.011.

Gradstein, F. M., J. G. Ogg, M. D. Schmitz, G. M. Ogg, eds., 2012, The geological time scale 2012: Elsevier, Amsterdam, p. 1176.

Handford, C. R., and R. G. Loucks, 1993, Carbonate depositional sequences and systems tracts—Responses of carbonate platforms to relative sea-level changes, *in* R. G. Loucks and J. F. Sarg, eds., Carbonate sequence stratigraphy: Recent developments and applications: AAPG Memoir 57, p. 3–41.

Haq, B. U., 2014, Cretaceous eustasy revisited: Global and Planetary Change, v. 113, p. 44–58, doi:10.1016/j.gloplacha.2013.12.007.

Hillgärtner, H., F. S. P. van Buchem, F. Gaumet, P. Razin, B. Pittet, J. Grötsch, and H. Droste, 2003, The Barremian-Aptian evolution of the eastern Arabian carbonate platform margin (northern Oman): Journal of Sedimentary Research, v. 73, no. 5, p. 756–773, doi:10.1306/030503730756.

Homewood, P. W., P. Maurland, F. Lafont, P. Sorriaux, Elf Exploration Production Predictive Stratigraphy Network, 2000, Best practices in sequence stratigraphy: For explorationists and reservoir engineers: Pau, France, Elf Exploration Production Memoir 25, 81 p.

Huck, S., U. Heimhofer, A. Immenhauser, and H. Weissert, 2013, Carbon-isotope stratigraphy of Early Cretaceous (Urgonian) shoal-water deposits: Diachronous changes in carbonate-platform production in the north-western Tethys: Sedimentary Geology, v. 290, p. 157–174, doi:10.1016/j.sedgeo.2013.03.016.

Huck, S., U. Heimhofer, N. Rameil, S. Bodin, and A. Immenhauser, 2011, Strontium and carbon-isotope chronostratigraphy of Barremian–Aptian shoal-water carbonates: Northern Tethyan platform drowning predates OAE 1a: Earth and Planetary Science Letters, v. 304, no. 3–4, p. 547–558, doi:10.1016/j.epsl.2011.02.031.

Hughes, G. W., 2000, Bioecostratigraphy of the Shu'aiba Formation, Shaybah field, Saudi Arabia: GeoArabia, v. 5, no. 4, p. 545–578, doi:10.2113/geoarabia0504545.

Immenhauser, A., H. Hillgärtner, U. Sattler, G. Bertotti, P. Schoepfer, P. Homewood, V. Vahrenkamp, et al., 2004, Barremian–lower Aptian Qishn Formation, Haushi-Huqf area, Oman: A new outcrop analogue for the Kharaib/Shu'aiba reservoirs: GeoArabia, v. 9, no. 1, p. 153–194, doi:10.2113/geoarabia0901153.

Kandel, D., 1992, Analyse paléotectonique de la plate-forme méridionale du bassin vocontien et de ses bordures, durant l'intervalle Barremo-albien (Ventoux-Lure-Baronnies, chaines subalpines méridionales, France), Ph.D. thesis, Université de Paris VI, Paris, 193 p.

Leenhardt, F., 1883, Etude géologique de la région du Mont-Ventoux, Doctoral thesis, Université de Montpellier, 273 p.

Léonide, P., J. Borgomano, J. P. Masse, and S. Doublet, 2012, Relation between stratigraphic architecture and multi-scale heterogeneities in carbonate platforms: The Barremian-Lower Aptian of the Monts de Vaucluse, SE France: Sedimentary Geology, v. 265–266, p. 87–109, doi:10.1016/j.sedgeo.2012.03.019.

Masse, J. P., 1976, Les calcaires urgoniens de Provence (Valanginien-Aptien inférieur). Stratigraphie, paléontologie, les paléoenvironnements et leur évolution, Ph.D. thesis, Université d'Aix Marseille II, Marseille, France, 445 p.

Masse, J. P., 1993, Valanginian to early Aptian carbonate platforms from Provence (SE France), *in* A. Simo, R. W. Scott, J.-P. Masse, eds., Cretaceous carbonate platforms. AAPG Memoir 56, p. 363–374.

Masse, J. P., S. Bouaziz, E. O. Amon, E. Baraboshin, R. A. Tarkowski, F. Bergerat, M. Sandulescu, J. P. Platel, J. Canerot, and R. Guiraud, 2000, Early Aptian (112–114 Ma), *in* J. Dercourt, M. Gaetani, and B. Vrielynck, eds., Atlas Peri-Tethys, Palaeogeographical Maps: CCGM, Paris, p. 119–127.

Masse, J. P., M. Fenerci, and E. Pernarcic, 2003, Palaeobathymetric reconstruction of peritidal carbonates: Late Barremian, Urgonian, sequences of Provence (SE France): Palaeogeography, Palaeoclimatology, Palaeoecology, v. 200, no. 1–4, p. 65–81, doi:10.1016/S0031-0182(03)00445-0.

Masse, J. P., and M. Fenerci-Masse, 2011, Drowning discontinuities and stratigraphic correlation in platform carbonates. The late Barremian/Early Aptian record of South-East France: Cretaceous Research, v. 32, no. 6, p. 659–684, doi:10.1016/j.cretres.2011.04.003.

Masse, J. P., and M. Fenerci-Masse, 2013, Drowning events, development and demise of carbonate platforms and controlling factors: The Late Barremian-Early Aptian record of Southeast France: Sedimentary Geology, v. 298, p. 28–52, doi:10.1016/j.sedgeo.2013.09.004.

Maurer, F., F. S. P. Van Buchem, G. P. Eberli, B. J. Pierson, M. J. Raven, P. H. Larsen, M. I. Al-Husseini, and B. Vincent, 2013, Late Aptian long-lived glacio-eustatic low stand recorded on the Arabian Plate: Terra Nova, v. 25, no. 2, p. 87–94, doi:10.1111/ter.12009.

McArthur, J. M., J. Mutterlose, G. D. Price, P. F. Rawson, A. Ruĵell, M. F. Thirlwall, 2004, Belemnites of Valanginian, Hauterivian and Barremian age: Sr-isotope stratigraphy, composition ($^{87}Sr/^{86}Sr$, $\delta^{13}C$, $\delta^{18}O$, Na, Sr, Mg), and palaeo-oceanography. Palaeogeography, Palaeoclimatology, Palaeoecology, v. 202, p. 253–272, doi:10.1016/S0031-0182(03)00638-2.

Michel, J., Lanteaume, C. Massonnat, G. Borgomano, J. Tendil, A. J. B. Bastide, F. Frau, et al., 2023, Questioning carbonate facies model definition with reference to the Lower Cretaceous Urgonian platform (SE France Basin): Bulletin de la Société Géologique de France, v. 194, no. 1, 13, 26 p., doi:10.1051/bsgf/2023009.

Moullade, M., G. Tronchetti, R. Busnardo, and J. P. Masse, 2000, Description lithologique des coupes types du stratotype historique de l'Aptien inférieur dans la région de Cassis e La Bédoule (SE France), in M. Moullade, G. Tronchetti, J. P. Masse, eds., Le stratotype historique de l'Aptien inférieur (Bédoulien, dans la région de Cassis - La Bédoule (S.E. France): Géologie Méditerranéenne, v. 26, p. 15–29.

Mutterlose, J., S. Pauly, and T. Steuber, 2009, Temperature controlled deposition of early Cretaceous (Barremian–early

Aptian) black shales in an epicontinental sea: Palaeogeography, Palaeoclimatology, Palaeoecology, v. 273, no. 3–4, p. 330–345, doi:10.1016/j.palaeo.2008.04.026.

Mutti, M., and P. Hallock, 2003, Carbonate systems along nutrient and temperature gradients: Some sedimentological and geochemical constraints: International Journal of Earth Sciences, v. 92, no. 4, p. 465–475, doi:10.1007/s00531-003-0350-y.

Pomar, L., and B. U. Haq, 2016, Decoding depositional sequences in carbonate systems: Concepts vs experience: Global and Planetary Change, v. 146, p. 190–225, doi:10.1016/j.gloplacha.2016.10.001.

Pomar, L., and W. C. Ward, 1995, Sea-level changes, carbonate production and platform architecture: The Llucmajor Platform, Mallorca, Spain, *in* B. U. Haq, ed., Sequence stratigraphy and depositional response to eustatic, tectonic and climatic forcing: Dordrecht, the Netherlands, Springer, p. 87–112.

Purdy, E. G., 1961, Bahamian oolite shoals, *in* J. A. Peterson and J. C. Osmond, eds., Geometry of sandstone bodies: AAPG Symposium, p. 53–62.

Rey, J., and P. Cugny, 1977, Ecoséquences et paléoenvironnements de l'Albien du Portugal: Bulletin de la Société d'Histoire Naturelle de Toulouse, v. 113, p. 374–386.

Sarg, J. F., 1988, Carbonate sequence stratigraphy, *in* C. K. Wilgus, B. S. Hastings, H. Posamentier, J. Van Wagoner, C. A. Ross, and C. G. St. C. Kendall, eds., Sea-level changes: An integrated approach: Tulsa, Oklahoma, SEPM Special Publication 42, p. 155–181, doi:10.2110/pec.88.01.0155.

Schlager, W., 1993, Accommodation and supply a dual control on stratigraphic sequences: Sedimentary Geology, v. 86, no. 1–2, p. 111–136, doi:10.1016/0037-0738(93)90136-S.

Schlager, W., 2005, Carbonate sedimentology and sequence stratigraphy: Tulsa, Oklahoma, SEPM Concepts in Sedimentology and Paleontology, v. 8, 200 p.

Sharland, P. R., R. Archer, D. M. Casey, R. B. Davies, S. H. Hall, A. P. Heward, A. D. Horbury, and M. D. Simmons, 2001, Arabian Plate sequence stratigraphy: Manama, Bahrain: GeoArabia Special Publication, v. 2, 371 p.

Tempier, C., and J. P. Durand, 1981, Importance de l'épisode d'âge crétacé supérieur dans la structure du versant méridional de la montagne Sainte-Victoire (Provence): Compte Rendu Académie de Sciences de Paris, v. 293, p. 629–632.

Tendil, A. J.-B., C. Frau, P. Léonide, F. Fournier, J. R. Borgomano, C. Lanteaume, J.-P. Masse, G. Massonnat, and J. P. Rolando, 2018, Platform-to-basin anatomy of a Barremian–Aptian Tethyan carbonate system: New insights into the regional to global factors controlling the stratigraphic architecture of the Urgonian Provence platform (Southeast France): Cretaceous Research, v. 91, p. 382–411, doi:10.1016/j.cretres.2018.05.002.

Tendil, A. J.-B., C. Frau, P. Léonide, F. Fournier, J. R. Borgomano, C. Lanteaume, J. P. Masse, and J. P. Rolando, 2019, Stable-isotope chemostratigraphy of Urgonian-type platform carbonates, Time to be cautious? *in* M. Montenari, ed., Stratigraphy & Timescales: New York, Academic Press, v. 4, p. 165–216.

Tucker, M., and V. P. Wright, 1990, Carbonate sedimentology: Oxford, United Kingdom, Blackwell, 482 p., doi:10.1002/9781444314175.

Weissert, H., and E. Erba, 2004, Volcanism, $CO_2$ and palaeoclimate: A Late Jurassic–Early Cretaceous carbon and oxygen isotope record: Journal of the Geological Society, v. 161, no. 4, p. 695–702, doi:10.1144/0016-764903-087.